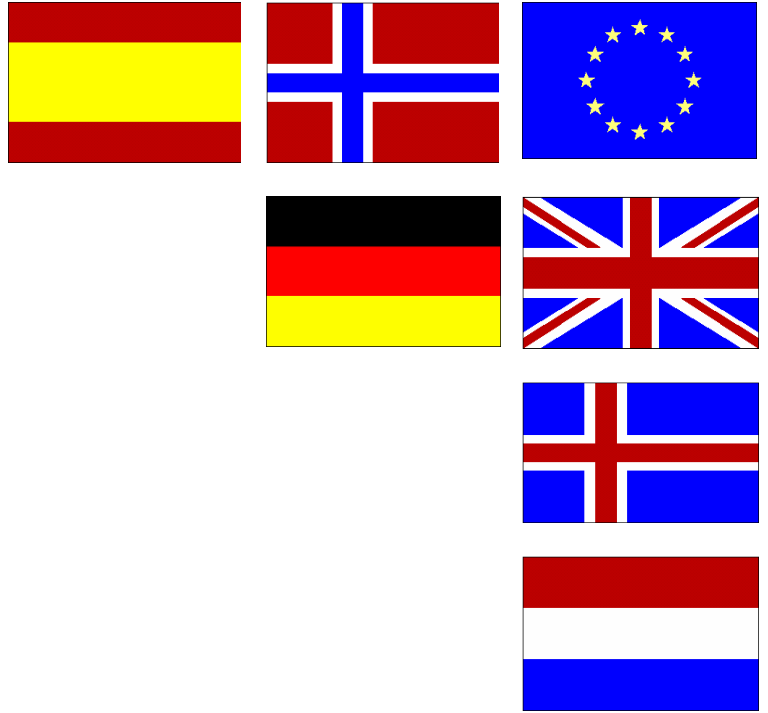


EuroLightCon



European Union – Brite EuRam III

The shear capacity of prestressed beams

EuroLightCon
Economic Design and Construction with
Light Weight Aggregate Concrete

Document BE96-3942/R42, June 2000

Project funded by the European Union
under the Industrial & Materials Technologies Programme (Brite-EuRam III)
Contract BRPR-CT97-0381, Project BE96-3942

The European Union – Brite EuRam III

The shear capacity of prestressed beams

EuroLightCon
Economic Design and Construction with
Light Weight Aggregate Concrete

Document BE96-3942/R42, June 2000
Contract BRPR-CT97-0381, Project BE96-3942

Although the project consortium does its best to ensure that any information given is accurate, no liability or responsibility of any kind (including liability for negligence) is accepted in this respect by the project consortium, the authors/editors and those who contributed to the report.

Acknowledgements

Wim Bennenk wrote this sub-task report 5.3.1. The report is based on the study of Stefan Droste and Marique Ruijs, junior researchers at the EUT. The author, Cees Kleinman, Harry Janssen and Sip Overdijk, the laboratory manager, coached both. Aleks Milenkovic and Math Pluis supported the study on behalf of Spanbeton. The tests are performed in the Pieter van Musschenbroek Laboratory of the EUT. The beams are produced by Hurks Beton B.V. in Veldhoven, NL. This report is a mutual effort of EUT and Spanbeton.

Information

Jan P.G. Mijnsbergen, CUR, PO Box 420, NL-2800 AK Gouda, the Netherlands

Tel: +31 182 540620, Email: jan.mijnsbergen@cur.nl

Information on the EuroLightCon-project and its partners: <http://www.sintef.no/bygg/segment/elcon>

ISBN 90 376 03 58 0

The European Union – Brite EuRam III

The shear capacity of prestressed beams

EuroLightCon
Economic Design and Construction with
Light Weight Aggregate Concrete

Document BE96-3942/R42, June 2000
Contract BRPR-CT97-0381, Project BE96-3942

Selmer ASA, NO
SINTEF, the Foundation for Scientific and Industrial Research at the
Norwegian Institute of Technology, NO
NTNU, University of Technology and Science, NO
ExClay International, NO
Beton Son B.V., NL
B.V. VASIM, NL
CUR, Centre for Civil Engineering Research and Codes, NL
Smals B.V., NL
Delft University of Technology, NL
IceConsult, Línuhönnun hf., IS
The Icelandic Building Research Institute, IS
Taywood Engineering Limited, GB
Lias-Franken Leichtbaustoffe GmbH & Co KG, DE
Dragados y Construcciones S.A., ES
Eindhoven University of Technology, NL
Spanbeton B.V., NL

Table of Contents

	PREFACE	7
	SUMMARY	11
1	INTRODUCTION	13
2	RESEARCH PERFORMED AT DELFT UNIVERSITY	14
3	THE DESIGN OF THE BEAM	16
3.1	Dimensions	16
3.2	Prestressing	17
3.3	Stirrups	18
3.4	Splitting tensile stresses	19
3.5	Torsion capacity of the beam	20
3.5.1	Capacity of the flanges	21
3.5.2	Torsional capacity of the box girder and the beam as a whole	22
3.5.3	Final longitudinal reinforcement	23
4	TEST ARRANGEMENTS	24
4.1	The test arrangement	24
4.2	Test specimens	25
4.2.1	The production of the beams, cubes and prisms	25
4.3	Applied materials.	26
4.4	Maturity, prestress release	27
4.5	Results of cube and prism tests	28
4.6	Prestressing force and time depending losses.	31
5	MEASURING PROCEDURES	32
5.1	Measuring procedure in the production stage	32
5.2	Measuring procedures for the shear force tests	33
5.3	Measuring procedure for the torsion test	34
5.4	Measuring procedure for the combined shear-torsion test	36
6	MEASURED RESULTS IN THE PRODUCTION STAGE	37
6.1	The measured transfer length of strands	37
6.1.1	The modification of the measuring procedure for some beams	37
6.1.2	The bond stress distribution along the strand	37
6.1.3	Measured transfer lengths	38

6.2	Slippage	41
6.3	Splitting tensile stresses	43
7	SHEAR FORCE CAPACITY OF THE BEAMS	44
7.1	Measured results analysed	44
7.1.1	Crack development	44
7.1.2	Deflection	44
7.1.3	Strains in the webs	46
7.1.4	Ultimate shear force capacity of the beams	46
8	TORSIONAL CAPACITY OF THE PRESTRESSED BEAMS	50
8.1	Measured results analysed	50
8.1.1	Crack development during the test	50
8.1.2	The torsional moment checked	50
8.1.3	Measured rotation	50
8.1.4	Measured strains	51
8.1.5	The torsional capacity of the beam	53
9	SHEAR AND TORSIONAL CAPACITY OF BEAMS	54
9.1	Measured results analysed	54
9.1.1	Crack development during the test	54
9.1.2	The torsional moment checked	55
9.1.3	Measured rotation	55
9.1.4	Measured strains	55
9.1.5	Flange bending and torsion	56
9.1.6	The ultimate capacity of the beam	60
10	PRESTRESSED LWA CONCRETE BEAMS	64
10.1	A new cross-section	64
10.2	The production of the beam	65
10.3	The test arrangements	66
10.4	Shear force test	68

PREFACE

The lower density and higher insulating capacity are the most obvious characteristics of LightWeight Aggregate Concrete (LWAC) by which it distinguishes itself from 'ordinary' Normal Density Concrete (NDC). However, these are by no means the only characteristics, which justify the increasing attention for this (construction) material. If that were the case most of the design, production and execution rules would apply for LWAC as for normal weight concrete, without any amendments.

LightWeight Aggregate (LWA) and LightWeight Aggregate Concrete are not new materials. LWAC has been known since the early days of the Roman Empire: both the Colosseum and the Pantheon were partly constructed with materials that can be characterised as lightweight aggregate concrete (aggregates of crushed lava, crushed brick and pumice). In the United States, over 100 World War II ships were built in LWAC, ranging in capacity from 3000 to 140000 tons and their successful performance led, at that time, to an extended use of structural LWAC in buildings and bridges.

It is the objective of the EuroLightCon-project to develop a reliable and cost effective design and construction methodology for structural concrete with LWA. The project addresses LWA manufactured from geological sources (clay, pumice etc.) as well as from waste/secondary materials (fly-ash etc.). The methodology shall enable the European concrete and construction industry to enhance its capabilities in terms of cost-effective and environmentally friendly construction, combining the building of lightweight structures with the utilisation of secondary aggregate sources.

The major research tasks are:

Lightweight aggregates: The identification and evaluation of new and unexploited sources specifically addressing the environmental issue by utilising alternative materials from waste. Further the development of more generally applicable classification and quality assurance systems for aggregates and aggregate production.

Lightweight aggregate concrete production: The development of a mix design methodology to account for all relevant materials and concrete production and in-use properties. This will include assessment of test methods and quality assurance for production.

Lightweight aggregate concrete properties: The establishing of basic materials relations, the influence of materials characteristics on mechanical properties and durability.

Lightweight aggregate concrete structures: The development of design criteria and -rules with special emphasis on high performance structures. The identification of new areas for application.

The project is being carried out in five technical tasks and a task for co-ordination/management and dissemination and exploitation. The objectives of all technical tasks are summarised below. Starting point of the project, the project baseline, are the results of international research work combined with the experience of the partners in the project whilst using LWAC. This subject is dealt with in the first task.

Tasks 2-5 address the respective research tasks as mentioned above: the LWA itself, production of LWAC, properties of LWAC and LWAC structures.

Sixteen partners from six European countries, representing aggregate manufacturers and suppliers, contractors, consultants research organisations and universities are involved in the EuroLightCon-project. In addition, the project established co-operation with national clusters and European working groups on guidelines and standards to increase the benefit, dissemination and exploitation.

At the time the project is being performed, a Working Group under the international concrete association FIB (the former CEB and FIP) is preparing an addendum to the CEB-FIP Model Code 1990, to make the Model Code applicable for LWAC. Basis for this work is a state-of-the-art report referring mainly to European and North-American Standards and Codes. Partners in the project are also active in the FIB Working Group.

General information on the EuroLightCon-project, including links to the individual project partners, is available through the web site of the project: <http://www.sintef.no/bygg/sement/elcon/>

At the time of publication of this report, following EuroLightCon-reports have been published:

- R1 Definitions and International Consensus Report. April 1998
- R1a LightWeight Aggregates – Datasheets. Update September 1998
- R2 LWAC Material Properties State-of-the-Art. December 1998
- R3 Chloride penetration into concrete with lightweight aggregates. March 1999
- R4 Methods for testing fresh lightweight aggregate concrete, December 1999
- R5 A rational mix design method for lightweight aggregate concrete using typical UK materials, January 2000
- R6 Properties of Lytag-based concrete mixtures strength class B15-B55, January 2000
- R7 Grading and composition of the aggregate, March 2000
- R8 Properties of lightweight concretes containing Lytag and Liapor, March 2000
- R9 Technical and economic mixture optimisation of high strength lightweight aggregate concrete, March 2000
- R10 Paste optimisation based on flow properties and compressive strength, March 2000
- R11 Pumping of LWAC based on expanded clay in Europe, March 2000
- R12 Applicability of the particle-matrix model to LWAC, March 2000
- R13 Large-scale chloride penetration test on LWAC-beams exposed to thermal and hygral cycles, March 2000
- R14 Structural LWAC. Specification and guideline for materials and production, June 2000
- R15 Light Weight Aggregates, June 2000
- R16 In-situ tests on existing lightweight aggregate concrete structures, June 2000
- R17 Properties of LWAC made with natural lightweight aggregates, June 2000
- R18 Durability of LWAC made with natural lightweight aggregates, June 2000
- R19 Evaluation of the early age cracking of lightweight aggregate concrete, June 2000
- R20 The effect of the moisture history on the water absorption of lightweight aggregates, June 2000
- R21 Stability and pumpability of lightweight aggregate concrete. Test methods, June 2000
- R22 The economic potential of lightweight aggregate concrete in c.i.p. concrete bridges, June 2000
- R23 Mechanical properties of lightweight aggregate concrete, June 2000
- R24 Prefabricated bridges, June 2000
- R25 Chemical stability, wear resistance and freeze-thaw resistance of lightweight aggregate concrete, June 2000

- R26 Recycling lightweight aggregate concrete, June 2000
- R27 Mechanical properties of LWAC compared with both NWC and HSC, June 2000
- R28 Prestressed beams loaded with shear force and/or torsional moment, June 2000
- R29 A prestressed steel-LWA concrete bridge system under fatigue loading
- R30 Creep properties of LWAC, June 2000
- R31 Long-term effects in LWAC: Strength under sustained loading; Shrinkage of High Strength LWAC, June 2000
- R32 Tensile strength as design parameter, June 2000
- R33 Structural and economical comparison of bridges made of inverted T-beams with topping, June 2000
- R34 Fatigue of normal weight concrete and lightweight concrete, June 2000
- R35 Composite models for short- and long-term strength and deformation properties of LWAC, June 2000
- R36 High strength LWAC in construction elements, June 2000
- R37 Comparison of bridges made of NWC and LWAC. Part 1: Steel concrete composite bridges, June 2000
- R38 Comparing high strength LWAC and HSC with the aid of a computer model, June 2000
- R39 Proposal for a Recommendation on design rules for high strength LWAC, June 2000
- R40 Comparison of bridges made of NWC and LWAC. Part 2: Bridges made of box beams post-tensioned in transversal direction, June 2000
- R41 LWA concrete under fatigue loading. A literature survey and a number of conducted fatigue tests, June 2000
- R42 The shear capacity of prestressed beams, June 2000
- R43 A prestressed steel-LWA concrete bridge system under fatigue loading, June 2000

SUMMARY

In this sub-task 5.1.3 of the EuroLightCon project the objective is to research the ultimate shear force capacity of prestressed beams with different concrete types and a high % stirrup reinforcement.

That means for the concrete types:

HSC, high strength concrete, concrete grade C105.

NWC, normal weight concrete, concrete grade C65.

LWAC, Lytag based Lightweight concrete, C55/C60.

That means for the loading history:

3 beams loaded with a shear force

3 beams loaded with a torsional moment

5 beams loaded with and shear force and torsional moment

The high % stirrup reinforcement indicates that the capacity of the concrete strut is tested. As long as an anchorage failure or a bending failure does not occur, the failure mode is failure of the compressive concrete strut.

The development of a LWA mix design with the application of Lytag, is one of tasks of Betonson, a well-known precast concrete company in the Netherlands. A mix design for C65 or higher, suitable for the precast concrete industry, was not yet completely ready, at the very moment the EUT project started. So it was decided to cut the EUT project in two stages.

In the first stage HSC and in the second stage LWAC and NWC, applied as reference.

The first stage is completely finished. The second stage started in the autumn of 1999 and is in progress. In this report the series of tests on prestressed HSC beams is completely documented and analysed. The beams for the test series on LWAC are designed and produced. The first tests on shear force are performed. Results of the work, done up till now, on the LWAC beams is reported separately in chapter 10.

The design of the test beam for the first series is strongly influenced by I-beam shape applied in tests at the Delft University of Technology on reinforced HSC beams, each provided with another % stirrup reinforcement. The objective of that research was to find a failure envelop on shear capacity versus % stirrup reinforcement.[3].

In the reported EUT project the aim is to test shear and torsion capacity of prestressed beams. To create torsional stiffness, the web of the I-beam is split into two parts. By creating a box girder inside the I-beam, the bending capacity did not change, the shear capacity did not change, but the torsional stiffness did.

The shear capacity is that high as expected. The compressive concrete strut failed explosively.

The torsional capacity was rather complicated to analyse. Besides torsion in the box part, there is also flange bending and flange torsion. As long as the beam is uncracked, applying the elastic theory can separate these effects. Due to cracking the shares of torsion and bending are changing. There has been developed a model, fitted to measured values, to describe the change of torsion to flange bending and flange torsion. The aimed failure mode was not achieved, because the web failed closer to the front of the beam. Although the ultimate capacity was not achieved, it was rather close.

For testing the capacity of the beams in the combination of shear and torsion, firstly the beams were loaded with a 25%, 50% and 75% of the torsional moment T_u . The beam rotates. Then the shear force is applied, while the torsional moment was kept constant.

Calculating according MC 90, the ultimate compressive stress in the strut for shear force and torsional moment ($f_{cT} + f_{cV}$) = $0.5 f_{cm}$. In which f_{cm} is the mean value of the compressive cube strength. For the shear capacity is valid $f_{cT} = 0.5 f_{cm}$.

The behaviour of the prestressed beam in a torsion test is not easy to describe. Due to crack development, a continuously change in stiffness and therefor the change in share of torsion and flange bending, it has been decided to modify the cross-section of the beam for the second series of tests. The beam is now a real box beam.

The first performed shear force tests on the prestressed LWAC box beams show other failure modes than expected.

Keywords

Prestressed beam, HSC, NWC,LWAC. Ultimate shear capacity, Shear force and/or torsional moment, Concrete strut failure.

1 INTRODUCTION

The Eindhoven University of Technology is involved in the EuroLightCon project in the sub-tasks 4 and 5, concerning material characteristics and structural applications. The material aspects and some structural aspects are reported in sub-task 4.2.4: The comparison of properties of LWAC, NWC and HSC.

Prestressed beams loaded with shear force and/or torsional moment are studied and tested in sub-task 5.3.1, to determine the ultimate shear capacity of the beams when a high percentage of stirrup reinforcement is applied. That means that the objective is, to let fail the concrete concrete strut in the cracked stage, while the stirrups do not yield. The crack development for non-prestressed and prestressed beams is different and the inclination of the crack will also differ. Does that influence the ultimate shear capacity?

For different types of concrete the ultimate shear strength can be compared. The objective is to apply HS-LWA concrete, a LWAC with a concrete grade = C65. The mix design of this HS-LWAC is a task for Betonson, one of the two Dutch precast companies in this Europe-wide project. The output of their task is the input for the EUT. However, at the start of the EUT – Spanbeton sub-task 5.3.1 the mix design was not yet available.

So, it was decided to start with the HSC beams directly and to wait until the mix design was available for a second series of tests.

Because some results of research at Delft University of Technology was available concerning the ultimate shear force capacity, which has directed the design of the test beam, to be able to compare the results optimally. The 90-mm web of the prestressed beam is split into two webs of 45 mm, to obtain torsional stiffness. The stiffness of the beam changes during the test continuously, so the interpretation of the results of the combined torsion – shear test is rather complicated.

The second stage of the project with LWAC beams and NWC beams, as reference, could start not earlier than October 1999. A change of the cross-section of the beam as well as the modification of test arrangements is discussed thoroughly and decided finally. The cross-section is now a box. A box beam is easier to evaluate as the I-shaped beam applied in the first stage of the project. All test beams are produced, the shear force tests on LWAC started in the second week of May 2000.

The precast prestressed concrete beams are manufactured by Hurks Beton BV, a very well known precast industry with its facilities close to the University. The reason to do this production is due the workload in the Laboratory with several projects in progress.

2 RESEARCH PERFORMED AT DELFT UNIVERSITY

In the orientation stage of the project, as much as possible literature has been studied. Design rules in the Codes are reviewed. In this report, especially the research performed at Delft University of Technology by Stroband, Walraven [3] is reviewed, because there exist a similitarity in the objective.

The shear force tests are performed on five I-shaped reinforced beams.

The total depth of the HSC beam $h = 700$ mm, the web thickness $b_w = 90$ mm.

The mean value of the concrete compressive cube strength $f_{cm,cube} = 115.8$ N/mm².

In each beam a different percentage of stirrup reinforcement -S500- is designed. The percentage of stirrup reinforcement is expressed as ratio of mm² reinforcement and the plain horizontal web cross-section. The longitudinal reinforcement also varied. The percentage stirrup reinforcement varies between 0.36% and 3.87%.

The test was designed, to check the design values for shear in the CUR Recommendation 37 concerning 'High Strength Concrete', written as an addition the Dutch Concrete Code VBC 1995/1995. Another interesting aspect is the angle θ , the angle between the concrete strut and the tie or bottom line of the beam, acting in failure stage or in design stage.

The beams are tested in an a-symmetrical three-point bending test. To avoid anchorage failure the longitudinal reinforcement is provided with a steel plate, which is welded to the rebars. The results of the tests are shown in Figure 1. The results indicate that an upper limit for the ultimate shear capacity is achieved with the application of 3.5% or 4.0% stirrup reinforcement.

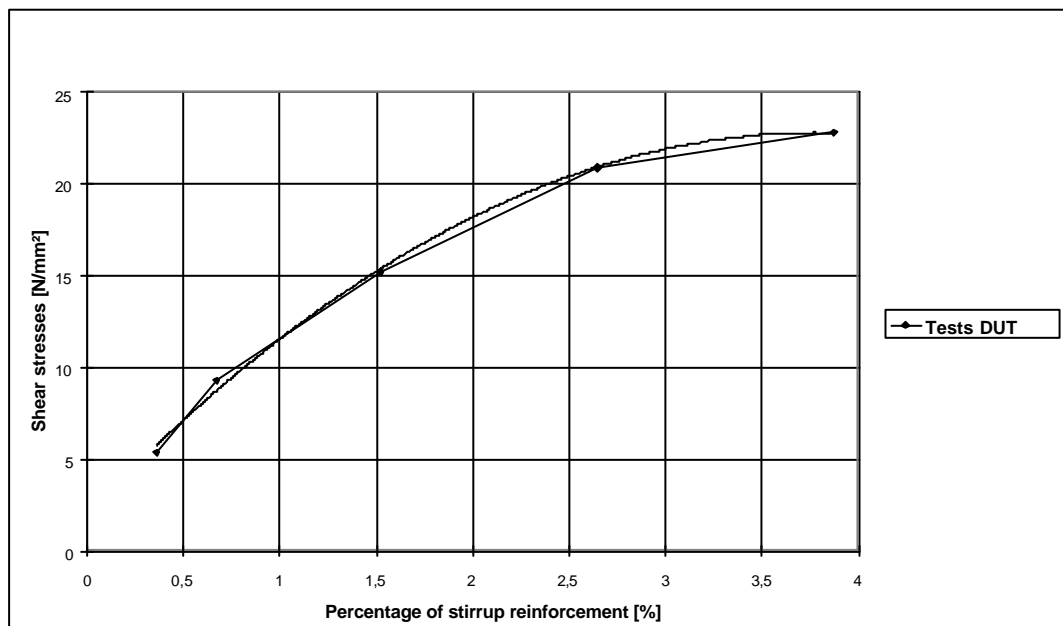


Figure 1 Shear force capacity related to the percentage of stirrup reinforcement, [3].

Conclusions of the performed research on reinforced beams are as follows:

- The inclination of the cracks in the web in the first stage of the test is $\pm 45^\circ$.
- For increased loading, more cracks do appear. The inclination decreases and specifically stronger when high stirrup reinforcement percentages are applied.
- The crack distance increases for higher stirrup reinforcement percentages.
- For low percentages the cracks are wider.
- With a limited strain of the stirrups, the capacity of the concrete concrete strut increases.
- $t_u = V_u / b.d = 0.2 \cdot f_{cm,cube}$ for stirrup reinforcement percentages $> 3.5\%$.

3 THE DESIGN OF THE BEAM

The objective is, to let fail the concrete compressive strut in the web of the beam. For a high percentage of applied stirrups this objective is feasible as long as bending failure does not occur. In the Dutch Concrete Code VBC 1995 the phenomena of such a shear failure is hidden in an upper limit value of t .

A shear force, a torsional moment or a combination of both causes the shear stress. The shear test is mostly performed as a three-point bending test with forces acting at $2.0 \cdot h_b$ or $2.5 \cdot h_b$ from one of the supports. The test for torsion is performed usually by introduction of the moment in the middle of the span or at the beam end. The support must be a fork type. Because no fixations can be made to the floor structure, a test set up with a torsional moment at the middle of the span is chosen.

3.1 Dimensions

Design and material parameters are:

Concrete grade	C 105
Prestressing steel	FeP 1860, $f_k = 12.9$ mm, $A_p = 100$ mm ² .
Reinforcing steel	FeB 500 or S 500
Span	$L = 7 h_b$ to $8 h_b$
Shear force	Force introduced at $2.0 h_b$ to $2.5 \cdot h_b$ from the support
Type of test	Three point bending test
Torsional moment	Moment acting at the middle of the span
Condition supports	Fork type

Mean shear stress according tests performed at the DUT is $t = \pm 22.8$ N/mm²

Mean value according a background document written by CUR $t = \pm 20.8$ N/mm².

According the formula in MC 1990:

$$V_{Rcw} = b_w \cdot z \cdot \cos q \cdot \sin q \cdot a \cdot f_{cm,cube} = t \cdot b_w \cdot d.$$

For the following assumptions a can be calculated:

$$\begin{aligned} t &= 23 \text{ N/mm}^2 \\ z &= 0.9 \cdot d \text{ (d is the structural depth)} \\ q &= 30^\circ \\ f_{cm,cube} &= 115 \text{ N/mm}^2 \text{ (mean compressive cube strength)} \end{aligned}$$

The result is: $a = 0.51$

It is at the safe side, to calculate in the pre-design with: $a = 0.6$ and $f_{cm,cube} = 115$ N/mm².

For the concrete strut to compressive stress $f'_c = 0.6 \cdot 115 = 69$ N/mm².

That means that the web thickness is of importance for the load to apply in the test.

The final dimensions for beam depth and web thickness is:

Web 90 mm thick. Beam 500 mm deep.

Jacket force acting at 1000mm from the support, at $2 \cdot h_b$.

An I profile does not show too much torsional stiffness, so it was decided to split the web of 90 mm into 2 x 45 mm. A part of the torsional moment will create real torsion in the shaped box-girder, but a part will also create torsion in the flange as well as flange bending. The web thickness is only 45 mm; for an applied stirrup $f 10$ the concrete cover is 17.5 mm. The designed beam is presented in Figure 2.

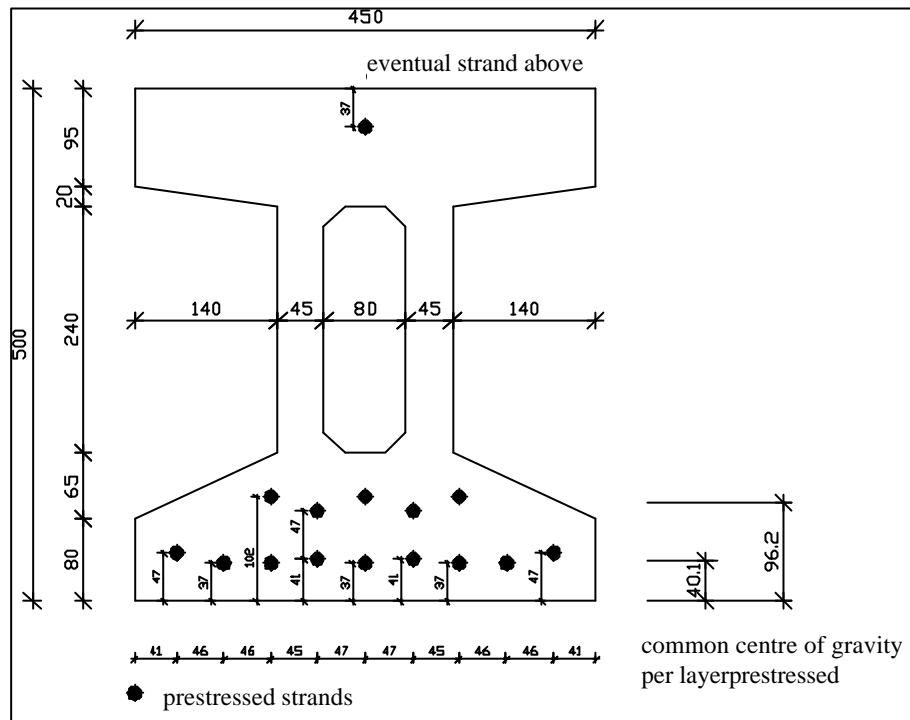


Figure 2 The designed cross-section of the prestressed HSC beam

3.2 Prestressing

$$V_u = b_w \cdot z \cdot \cos \alpha \cdot \sin \alpha \cdot a \cdot f_{cm,cube} = t \cdot b_w \cdot d.$$

$$V_u = t \cdot b_w \cdot d = 23 \cdot 90 \cdot 0.9 \cdot 500 \cdot 10^{-3} = 932 \text{ kN}.$$

$$M = V_u \cdot 2 \cdot h = 932 \cdot 2 \cdot 0.5 = 932 \text{ kNm}$$

In the bottom flange 14 strands, $f 12.9$; $A_p=100 \text{ mm}^2$ are applied.

Due to the prestress force on the bottom flange, the bending tensile stresses at the topside are in the range of 7 N/mm^2 , so rather high. So, some additional prestressing in the top flange is required; chosen is to prestress 1 $f 12.9$ strand. The strands are positioned at three levels of depth.

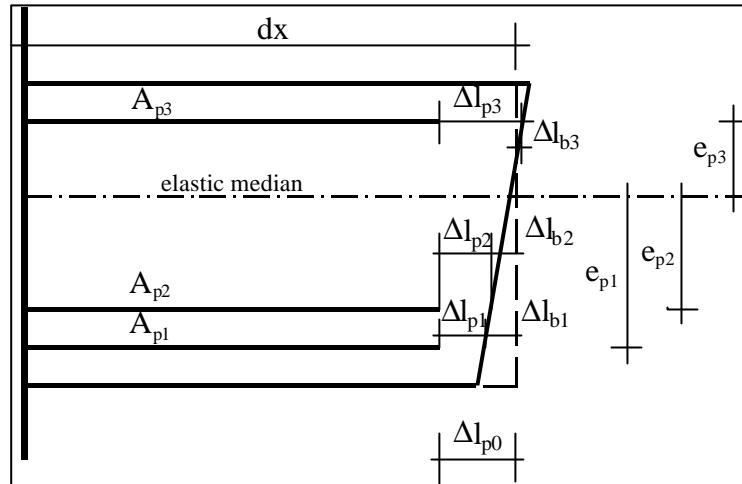


Figure 3 Principle to determine the prestress stresses after prestress release.

The initial prestressing stress is 1450 N/mm². It is assumed that $f_{cm} = 65 \text{ N/mm}^2$ at prestress release. After losses, due to elastic deformation, the following prestress forces are left:

$F_{p01} = 1305 \text{ KN}$	$F_{pi1} = 1157 \text{ KN}$	$F_{pi1} / F_{p01} = 88.7\%$
$F_{p02} = 725 \text{ KN}$	$F_{pi2} = 654 \text{ KN}$	$F_{pi2} / F_{p02} = 90.2\%$
$F_{p03} = 145 \text{ KN}$	$F_{pi3} = 145 \text{ KN}$	$F_{pi3} / F_{p03} = 100.4\%$
	$F_{pi \text{ tot}} = 1957 \text{ KN}$	

The stresses in the concrete are:

$$s_{cb} = -34.7 \text{ N/mm}^2. \quad s_{ct} = +3.9 \text{ N/mm}^2 < 4.7 \text{ N/mm}^2.$$

The centre of gravity of the prestressing force is situated at 90.7 mm from the bottom side of the beam.

3.3 Stirrups

According MC 1990, the influence of the prestressing stress - acting in the concrete strut direction - is taken into account when calculating the stirrup reinforcement.

$$s'_c = \frac{F_{pitot}}{A_{bn} (1 + \tan^2 \theta)}$$

In Figure 4 the direction is showed graphically.

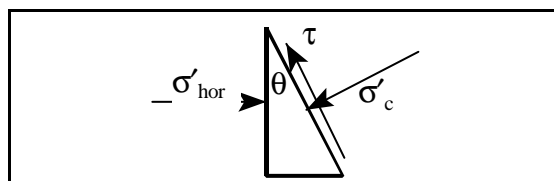


Figure 4 Mean value of the concrete compressive stress in concrete strut direction.

$F_{pi \text{ tot}} = 1957 \text{ kN}$	
$A_{cn} = 126000 \text{ mm}^2$	exclusive the contribution of non-prestressed reinforcement.
$\theta = 30^\circ$	
$s'_c = 11.6 \text{ N/mm}^2$	

$$V_{Rcw} = b_w \cdot z \cdot \cos \alpha \cdot \sin \alpha \cdot a \cdot (f_{cm,cube} - s \cdot c)$$

$$V_{Rcw} = 90 \cdot 0.8 \cdot 500 \cdot \cos 30 \cdot \sin 30 \cdot (0.6 \cdot 115 - 11.6) \cdot 10^{-3} = 895 \text{ kN.}$$

Due to the time-dependent deformations, (shrinkage, creep and relaxation), the prestress force will decrease, so V_{Rcw} will increase.

The stirrup reinforcement per mm¹ beam:

$$A_{sw} > V_{Rcw} / (f_{yd} \cdot z (\cot \alpha + \cot \beta)) = 895000 / (435 \cdot 0.8 \cdot 500 (\cot 30 + 0)) = 2.97 \text{ mm}^2/\text{mm}^1$$

This means: $f_{12} - 76 \text{ mm}^1$ or $f_{10} - 53 \text{ mm}^1$. The choice is $f_{10} - 50 \text{ mm}^1 = 316 \text{ mm}^2$.

The ultimate tensile stress of the reinforcing steel will exceed 500 N/mm², so some additional reserve is built in.

$$V_{Rcw} = 1.15 (3.16/2.97) \cdot 895 = 1095 \text{ kN.}$$

$$t = V_u / b_w \cdot d = 1095000 / (90 \cdot 440) = 27.7 \text{ N/mm}^2.$$

In Figure 5 the shape of the stirrups is shown. The stirrup is built from two identical parts, spot welded together locally for fixation reasons.

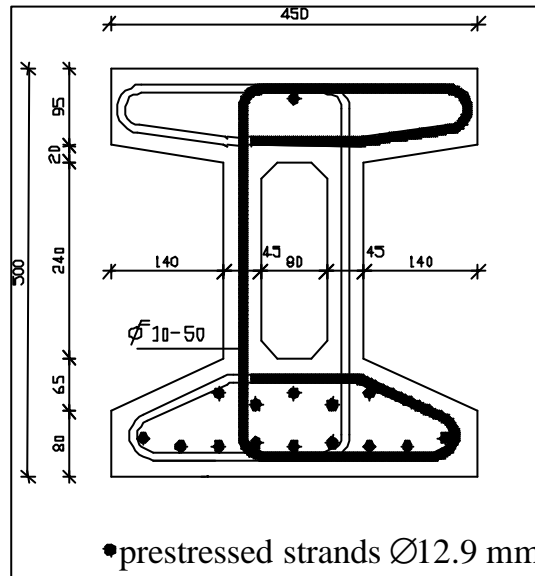


Figure 5 Cross-section of the beam provided with the stirrup reinforcement.

3.4 Splitting tensile stresses

The splitting tensile stresses are calculated with a replaced prism, a common method, but also with a FEM package Lusas. According both applied methods, the tensile stresses are too high. A reduction of the effective prestressing force is possible by debonding some strands at the end of the beam over a certain length. However, the absence of prestressing is possibly leading to anchorage failure when the concrete strut force is as high as estimated on forehand; not an attractive solution in this particular situation. So, it has been decided, to provide the beam with a hammer end, over 150 to 250 mm. The web thickness is doubled to 2 x 90 mm; some additional stirrups are applied.

The length of the hammer end is 250 mm, as long as the cantilever of the beam during the test. The transfer length of the strands probably 350 mm, so anchorage failure is not expected.

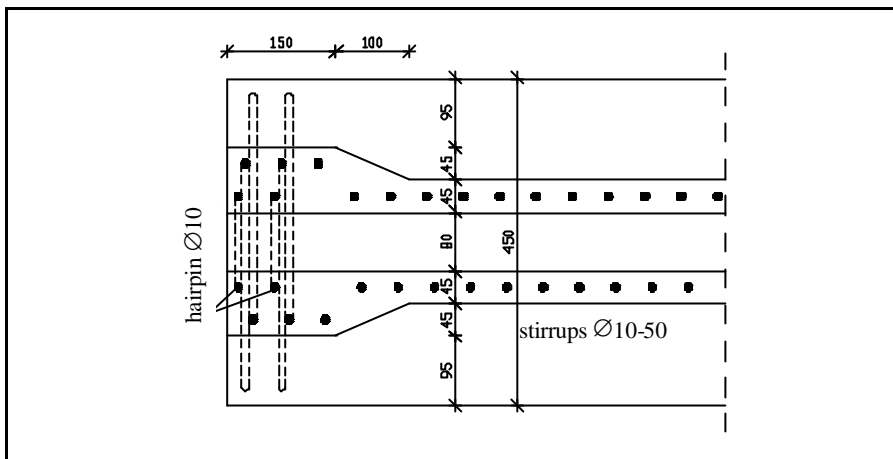


Figure 6 Detail of the hammer end of the beam.

3.5 Torsion capacity of the beam

Due to the decision to apply a torsional moment in the middle of the span of the beam, no pure
The formula can be applied to determine the ratio of flange bending. :

$$\frac{d\phi}{dx} = \frac{T_{wr} - V_y \cdot h}{G \cdot I_{wr}} \quad (1)$$

The boundary conditions are:

The front of the beam at the support is a plane: for $x = L$ $df/dx = 0$.

When not, the flanges rotate in different directions: for $x = L$ $df/dx \neq 0$.

$x = 0$ the middle of the span of the beam

$x = L$ the support, so L is distance from the middle to the support.

The designed beam is provided with a hammer end and is supported 250 mm from the front of the beam, see Figure 7 for the horizontal cross section.

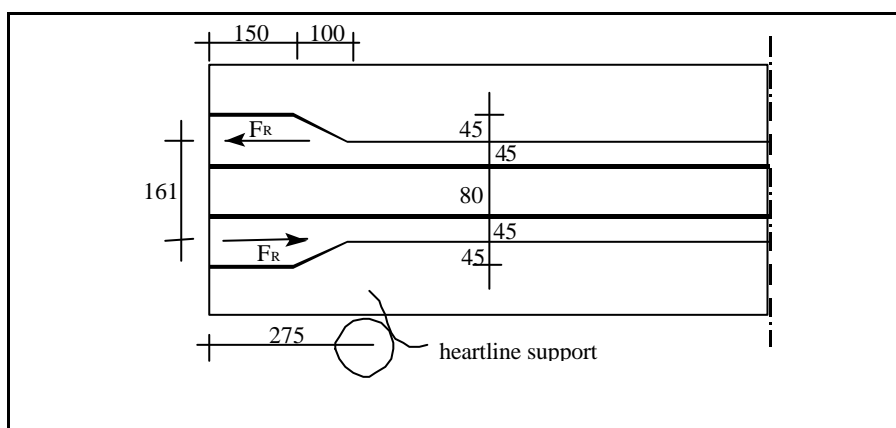


Figure 7 Horizontal cross-section at the support zone of the beam.

The boundary conditions do also change when cracking starts in the end zone. So, two different limits are reviewed:

Case 1: $x = L$? $df/dx = 0$:

At	$x = 0$?	$df/dx = 0$	(symmetry reasons)
At	$x = L$?	$df/dx = 0$	(assumed to be clamped in)
At	$x = L$?	$f = 0$	(the support does not rotate)

For the location where the torsional moment is introduced, (the axis of symmetry) and at the end of the beam, a clamped in situation is assumed, that means:

For	$x = L/2$?	$M_{flange} = 0$.
For	$x = L/2$?	$d^2f/d^2x = 0$.

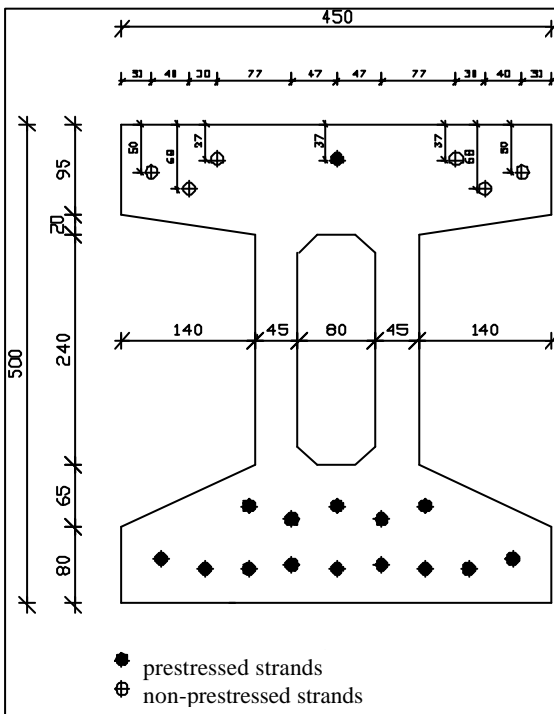
Case 2: $x = L$? $df/dx \neq 0$:

At	$x = 0$?	$df/dx = 0$.	(symmetry reasons)
At	$x = L$?	$f = 0$.	(no rotation at the support)

For	$x = L$?	$M_{flange} = 0$.
For	$x = L/2$?	$d^2f/d^2x = 0$.

The differential equation can be solved for both boundary conditions. The share of flange is thereby indicated, because the formula is only valid for the uncracked stage.

3.5.1 Capacity of the flanges



In the top flange is 1 prestressed strand \varnothing 12.9 mm present. The strand is positioned in the middle of the flange. Due to flange bending, reinforcement in longitudinal direction is needed to resist the bending effects and to limit cracking. Decided is to apply the same strands as applied for prestressing, but now non-prestressed. Per flange-tip 3 strands \varnothing 12.9 mm.

The bottom flange is heavily prestressed, so bending effects will there be eliminated by the acting compressive stresses. The position of the strands is shown in Figure 8.

Figure 8 Necessary additional reinforcement, due to flange bending.

3.5.2 Torsional capacity of the box girder and the beam as a whole

First of all, the torsional capacity of the box part will be reviewed according MC 1990.

$$F_{S_{wi}} = V_{s_{di}} / \sin \alpha_i$$

$$F_{R_{wi}} = f_{cd2} t_i z_i \cos \alpha_i \quad (\text{capacity of the concrete strut})$$

Unknown are: $f_{cd2} \text{ en } \cos \alpha_i$. In MC 1990 the value of f_{cd2} is the same for shear as for torsion. However, the compressive stress of the concrete strut for shear is uniformly distributed over the cross-section, while due to torsion, the stresses at the outside of the cross-section are higher. In the calculation for $F_{R_{wi}}$ the same upper limit for the compressive stress in the concrete strut is applied; the angle of the concrete strut is $\alpha_i = 30^\circ$.

Due to the mean compressive stress in the direction of the concrete strut, a capacity of $(69-11.6) = 57.4 \text{ N/mm}^2$ is left.

$$F_{R_{wi}} = 57.4 \cdot 45 \cdot 436.6 \cdot \cos 30^\circ \cdot 10^{-3} = 977 \text{ kN per web of 45 mm.}$$

$$V_{s_{di}} = 977 \cdot \sin 30^\circ = 498 \text{ kN. (1)}$$

For the box girder within the cross-section of the beam:

$$T_u = 2 \cdot 498 \cdot 0.125 \cdot 0.915 = 114 \text{ kNm.}$$

$$t_{ti} = V_{s_{di}} / (z_i \cdot t_{\text{eff}}) = 498000 / (436.6 \cdot 45) = 25.3 \text{ N/mm}^2.$$

Considerations:

Due to flange bending, the upper flange will show cracks; the stiffness of the flange will decrease. In the bottom flange the bending tensile cracks will appear in a later stage of the test, because the prestressing is causing compressive stresses.

The crack development in the upper flange will progress, due to shear stresses, caused by the torsional moment acting in the box girder section. In the next stage the web will separate from the upper flange, followed by the separation of the bottom flange.

Because the flanges do not crack at the same stage of the torsion test, the stiffness of the flanges is not equal, so the centre of gravity of the cross-section will change, secondary effects will act next to pure torsion. The change of stiffness means also the change in the ratio torsion, flange bending and flange torsion.

So, one has to be aware that:

- Both the torsional stiffness and the bending stiffness decrease when the torsional moment increases.
- By crack development in the box girder part of the beam, the bending stiffness of the flanges will decrease.
- The share of flange bending, flange torsion is not easy to determine, due to the continuously changing stiffness of parts.

We assume:

$$\begin{aligned} T_u - \text{torsion in box girder} - &= 114 \text{ kNm} \\ M_u - \text{flange bending} - &= 193 \text{ kNm} \end{aligned}$$

A detailed study [1] shows that the torsional moment capacity will increase to:

$$T_u - \text{total moment} - = 140 \text{ kNm per cross-section.}$$

To apply in the test $2.140 \text{ kNm} = 280 \text{ kNm}$ in the middle of the span.

3.5.3 Final longitudinal reinforcement

The lever arm of the load cells at the support is 412 mm. So the load cell will be loaded with $V_d = 140 / 0.412 = 340 \text{ kN}$. The applied stirrup reinforcement is able to resist the shear force. The prestressing force is acting in the bottom flange, therefore no additional reinforcement in the bottom flange is needed to resist the effects of torsion in the box girder. In the top flange 4 non-prestressed strands $\varnothing 12.9 \text{ mm}$ are positioned as longitudinal reinforcement. The final number of strands is shown in Figure 9.

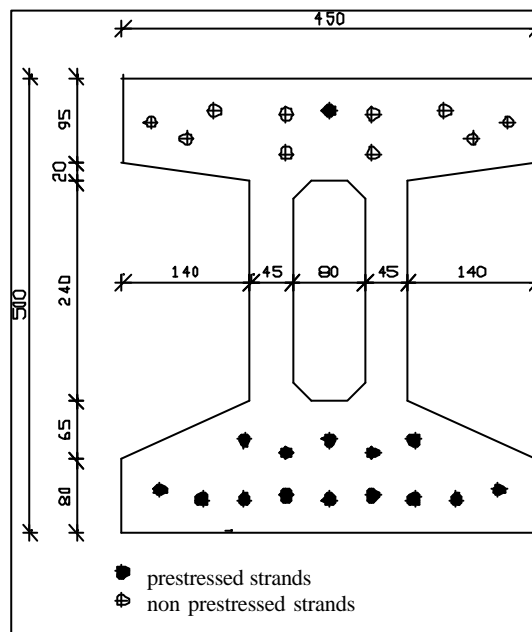


Figure 9 Reinforcement in the cross-section

4 TEST ARRANGEMENTS

In Figure 10 the designed test beam is presented. The stirrup reinforcement is ϕ 10-50 mm. In total 12 HSC beams are produced; for the shear force test 3, for the torsion test 3 and for the combination of both 5 and 1 as spare.

The beams are produced in the factory of Hurks Beton B.V in Veldhoven, close to the EUT, by the researcher and laboratory staff of EUT. The reasons to decide for an outside production are:

- The capacity in space, because several projects are running at the same period of time and
- The limited volume of the laboratory concrete mixer.

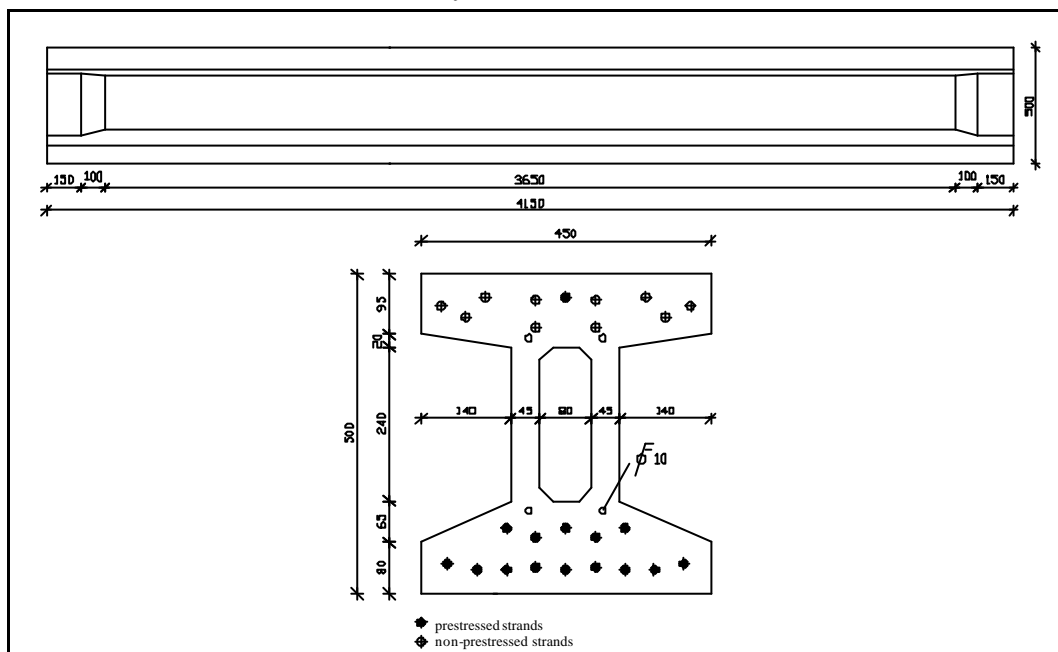


Figure 10 Dimensions of the test beam

4.1 The test arrangement

The test arrangement is shown in Figure 11. The frame is constructed of steel beams fitting to a modular 300 mm fixing system with bolts. The distance between the supports is 3600 mm. The force is introduced at 1.0 metre from the support for the shear force test and at 1.8 m for the torsion test. The modifications of the test arrangement for torsion are made after the shear test is finished.

In the shear test, 2 jackets with 1000 kN capacity, are applied. In the torsion test, 2 eccentrically positioned jackets of 300 kN - at a distance of 1.5 metre c.o.c are applied. The total arrangement is not fixed to the floor, so the stability has to be achieved within the arrangement itself. The beams are connected to each other with bolts M24 10.9.

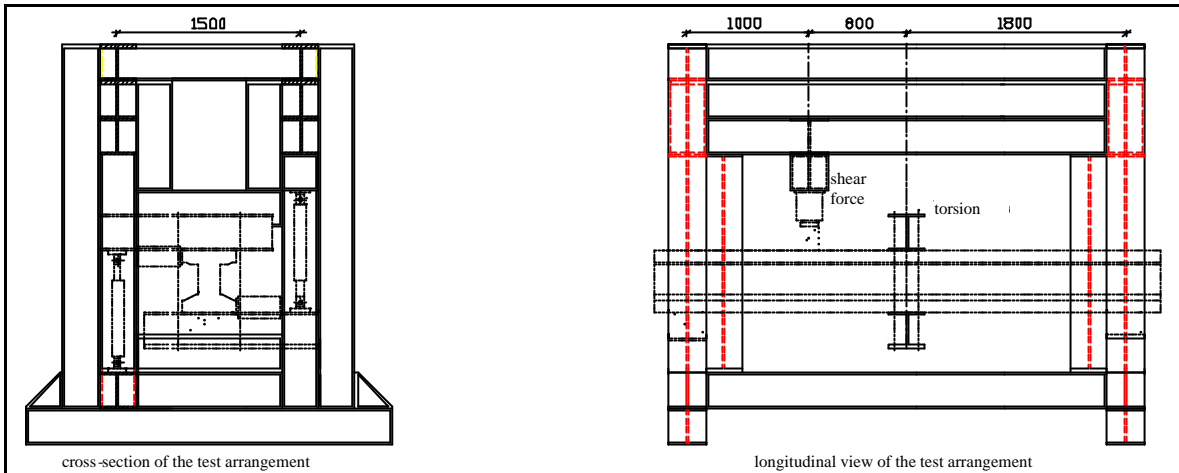


Figure 11 Test arrangement.

4.2 Test specimens

4.2.1 The production of the beams, cubes and prisms

The beams are cast in a timber mould provided with steel end closures, to arrange the accurate position of the strands in the cross-section, see Figure 12. The compaction of the concrete is realised with 3 vibrators, fixed under the bottom side of the mould. To shape the hollow core, plates of roofmate are glued together. In the middle of the foam core two holes are left for small pipes, in which 2 strands are pushed. The strands are prestressed up to 80 kN before the casting operation starts, to keep the foam at the correct location.

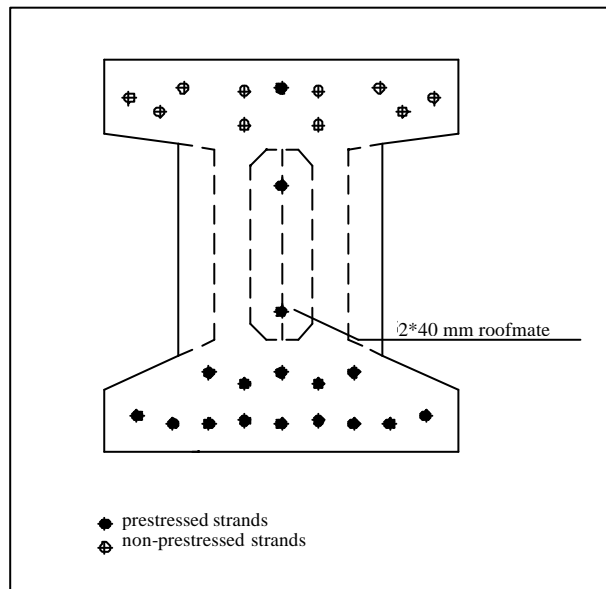


Figure 12 Steel end closure and the positioning, fixation, of the roofmate core

The strands are prestressed up to 120 kN and in the same sequence stressed up to the required 145 kN. The effective prestressing force in the steel will be some lower than the 145 kN, which

is in fact the jacket force, just before blocking the strand. The loss of stress is due to the slippage in the wedge.

In the casting operation the following test specimens are produced:

- 8 cubes 100 x 100 x 100 mm³.
- 10 cubes 150 x 150 x 150 mm³.
- 3 prisms 100 x 100 x 500 mm³.

Six cubes with sides of 150 mm are stored under water to check the 28-days and 56-days strength. It is expected that after the hardening period of one month, the strength increase is still substantially. The hardening is not accelerated; no heat is added after casting.

The other test specimens are stored next to the beams, under a plastic sheet.

4.3 Applied materials.

The concrete mix design for HSC grade C 105 is based on the mix design, as applied in the HSC research project of Paul Vossen, performed at the EUT[2].

Table 1 Mix composition

Constituent materials per 1000 litre.	Weight [kg]
Sand 0-4 mm	762
Split gravel 5-11 mm	743
Split gravel 8-16 mm	353
Cement Anneliese CEM I 52.5 R	475
Water (w.c.r. = 0.28)	107
Silica slurry (50% is water)	52.25
Superplasticizer FM 951 (3% of the cement mass)	14.25

In the Table the weight of the dry material is shown, except for the slurry. The water in the slurry is taken in account for the total amount of water applied.

Prestressing steel.

The E-modulus of the prestressing strands FeP 1860 is tested on wires from the mid-section of 3 strands.

The mean value $E_{p,m} = 210371 \text{ N/mm}^2$ ($s_3 = 2053 \text{ N/mm}^2$).

De mean value of the tensile stress = 1937 N/mm^2 .

In the calculation is used $E_p = 200000 \text{ N/mm}^2$, which is normal for the strand itself.

The diameter of the middle wire and others is measured, measuring accuracy 0.001 mm.

The ratio -diameter middle wire / diameter outside wire- is respectively: 1.05, 1.04 en 1.04. According NEN 6008 the ratio has be between 1.02 and 1.05, so the strands meet the requirements.

Reinforcement FeB 500 HKN.

The E-modulus following from the s-e diagrams of 3 rebars is:

$$E_{s,m} = 194454 \text{ N/mm}^2. (s_3 = 4466 \text{ N/mm}^2)$$

The ultimate tensile stress is: 591 N/mm^2 .

In the calculations is used: $E_s = 200000 \text{ N/mm}^2$.

4.4 Maturity, prestress release

The relationship of maturity versus compressive cube strength is determined at Hurks Beton.

To prestress the beam up to 34.7 N/mm^2 , the actual compressive cube $f'_{c,cube}$ has to be at least $34.7/0.6 = 58 \text{ N/mm}^2$. In general the mean value for the cube strength $f'_{cm,cube}$ will be 65 N/mm^2 .

The measured maturity has to be beyond $550 \text{ }^\circ\text{Ch}$.

Thermocouples are positioned inside the bottom flange of the beam and connected with the maturity computer, activated just after casting is finished.

The maturity is calculated as follows:

$$R_g = 10.(C^{(0.1.T-1.245)} - C^{(-2.245)}) / \ln C [^\circ\text{C.h}] \quad (\text{The start value } C \text{ for Anneliese cement } = 1.3)$$

To determine the compressive strength of the concrete at prestress release, the mean value of the maturity in the bottom flange, the upper flange and the web is chosen as representative one.

The equation is:

$$f_{ct} = -286.538 + 128.205 \log(R_g)$$

In Table 2 the actual compressive cube strength at prestress release is shown.

Table 2 The actual compressive cube strength with the belonging maturity

Beam #	1	2	3	4	5	6	7	8	9	10	11	12
$R_{g,m}$	678	554	716	542	611	543	584	740	790	576	656	1024
f_{ct}	76	65	79	64	71	64	68	81	85	67	75	99

To check, whether the relationship is still valid for the next casting operation, 1 cube is provided with a thermocouple, stored with the other cubes, covered with a plastic sheet.

When its maturity is close to $550 \text{ }^\circ\text{Ch}$ the cube is pressed. Due to temporarily technical problems a check via a temperature controlled water basin was not possible. Normally the temperature in the basin is controlled and steered via a thermocouple positioned in the beam. In fact, the temperature in the basin, is normally identical to the measured temperature in the beam. The beam is stored outside, some hours after the prestress release is performed.

The control cubes and prisms are sent to the EUT 24 hours after casting and in the Pieter van Musschenbroek Laboratory stored under water, so in fact, the strength development will deviate from the beam's one.

4.5 Results of cube and prism tests

More than one beam is produced in one shift, so at the test date the age of the beams are different. Therefore three cubes $100 \times 100 \times 100 \text{ mm}^3$ are tested after 28-days, to learn whether there are substantial differences in the strength of the beams.

The other cubes and prisms are tested at the testing date.

As mentioned previously, 6 cubes with sides of 150 mm are stored under water. Three of 6 are tested at 28 days of age and the other 3 at 56 days of age. In Table 3 the results of tests at 28 days are presented.

Table 3 Cube strengths at 28 days, EUT (100mm) and Hurks at 56 days (150 mm)

Beam	1	2	3	4	5	6	7	8	9	10	11	12
$f_{cm\ 100}$	110. 7	112.0	119.1	116.6	107.8	114.8	111.7	113.6	101.8	109.8	116.9	118.6
$f_{cm\ 150}$	104. 6	118.1	120.8	114.7	114.7	103.8	106.2	-----	106.3	115.8	111.1	114.1
f_{150}/f_{100}	0.94 5	1.055	1.015	0.983	1.064	0.904	0.951	-----	1.044	1.055	0.951	0.962

For 11 of 12 beams, the mean value of $f_{cm\ 150}/f_{cm\ 100} = 0.993$ and $s = 0.055$.

In [12] the correlation factor is 0.98 and in [5] a correlation factor of 0.95 is found. In the Dutch code is indicated a factor of 0.91. Although between cube tests on cubes with 100 mm sides and 150 mm sides, small differences are found, a correlation factor equal to 1 is acceptable.

Reference data:

The concrete compressive stress of the beams is measured at 5 cubes $100 \times 100 \times 100 \text{ mm}^3$. The deformation speed is 1 mm/min. The cube is tested at the test date of the beam. The mean values of the cube compressive tests are presented in Table 4.5.1.

The splitting tensile stress is measured at 3 cubes $150 \times 150 \times 150 \text{ mm}^3$. The deformation speed is 1 mm/min. The splitting tensile stress $f_{cts} = 2.F/(p.150^2)$. Results are presented in Table 4.5.1.

The uniaxial tensile strength is not known. In CUR-Report 93-7[19], it is written that f_{ct} is 70% of the measured splitting tensile strength is the uniaxial tensile strength. This rate is adopted. Results are presented in Table 4.5.1.

The bending tensile strength is measured in a -three points- bending test. Prisms $100 \times 100 \times 500 \text{ mm}^3$ are applied for such a test. The deformation speed is 0.6 mm/min. In the contact zone, under the jacket, on the top of the prism a piece of soft board is used, to avoid peak stresses.

The depth of the beam is 0.5 m. The depth of the prism 0.1 m. The influence of the depth of the beam is: $f_{cr}(\text{beam}) = f_{cr}(\text{prism}).(1.6 - 0.5) / (1.6 - 0.1) = f_{cr}(\text{prism})/ 1.364$. According the Dutch Concrete Code VBC 1995, the mean value for the tensile stress can be calculated by $f_{cm} = f_{cm}(\text{prism})/1.5$. The results from this relationship are higher than the calculated value of f_{ct} .

The shear capacity of prestressed beams

The E-modulus is measured for 3 prisms $100 \times 100 \times 500 \text{ mm}^3$. The loading is limited to $2/3$ of the estimated compressive stress of the prisms. The stress is approximately 60 N/mm^2 . The deformation speed is 0.139 mm/min . The measured results are presented in Table 4.5.1. After measuring the E-modules, the 3-points bending test is performed at the same prism.

The final calculations are based on the data, presented in Table 4.

Table 4

4.6 Prestressing force and time depending losses.

It is important to know the magnitude of the prestressing force rather accurate, at the test date of the beam. For the losses, due to creep and shrinkage of concrete, the following formula is used:

$$\Delta\sigma_{pkr} = \sigma_{bp}(0) \cdot n_e \cdot \phi + \varepsilon'_r(t) \cdot E_p$$

The relaxation of the prestressing steel is normally 3 times as high at t=50 years as at 1000 hours, the duration of the relaxation test. The beams are tested on shear at say 40 days = ± 1000 hours. So the relaxation factor 3 will be neglected for shear. The formula to calculate the relaxation is:

$$\Delta\sigma_p = \Delta\sigma_{prel} \left(1 - 2 \frac{\Delta\sigma_{pkr}}{\sigma_{pi}} \right)$$

However, when the torsion test and shear -torsion test is performed, the beams are older of age, so the value of 3 for the long-term influence is applied in these test data.

5 MEASURING PROCEDURES

5.1 Measuring procedure in the production stage

In Figure 13, all measuring points are presented. In this part of the report, several aspects are reviewed, such as:

- Temperature and maturity.
- Transfer length and slippage of the strands.
- Camber.

Temperature and maturity

To learn the ambient conditions, both the temperature and the relative humidity are measured during the production stage within the factory.

Thermocouples are installed at three locations in the beam, to monitor the temperature in the beam. The thermocouples are connected with the maturity computer. The differences between the top and bottom flange are also registered because these differences are responsible for camber development after the cooling down period.

Transfer length and slippage of the strands.

The real prestressing force is measured digitally before the strand is anchored. The prestressing force is 145 kN, just before anchoring the strand. However, the real stress in the strand is not known, because the slippage during pushing the wedges in position in the anchor is different for each strand in principle. At the passive side, the side where the strand is anchored on forehand, two load cells are fixed to two strands to register the force in the strand.

The force in the jacket at prestress release is also measured. The release of the prestressing force is divided into five stages.

During the prestress release the changes of the distances between the measuring points, all glued at the sides of the beam, are measured manually with a Pfender meter. The measurements are accurate up to 0.001 mm. The change in strain is equal to the measured change in distance divided by the original distance.

The points are glued at the 2 sides of the beam at a depth equal to the centre of gravity of the strands in the bottom flange. The distance between two points is 60 mm. The mean value of the change in deformation at both sides is taking into account. The deformation is measured over a length of 9 x 60 mm, to learn where the prestressing force is transferred.

In the middle of the span the vertical displacements are measured, as performed at the ends of the beam. The points are glued at the side of the bottom flange as well as at the side of the top flange. The objective is, to check the strain-stress situation in the middle of the beam.

The slippage of the strands is measured by 4 LVDT's fixed on the strands at both ends of the beam. The measuring accuracy with LVDT's is 0.001 mm. The strain of the part of the strand between the front of the beam and the LVDT has to be taken into account.

- The strains at the bottom side of the beam are measured with LVDT's, to enable the researcher to continue the measuring procedure after cracking.
- On the outside surface of the web, the strains are measured in three directions. These special strain gauges are placed in a straight line, under 45° with the beam axis in longitudinal direction. By measuring the strains in three directions, it is possible to calculate the principle stresses from these strains. The influence of cracks will be shown clearly in the registered data. The roofmate core is removed before the test starts.
- The jacket force is measured to learn the acting torsional moment.

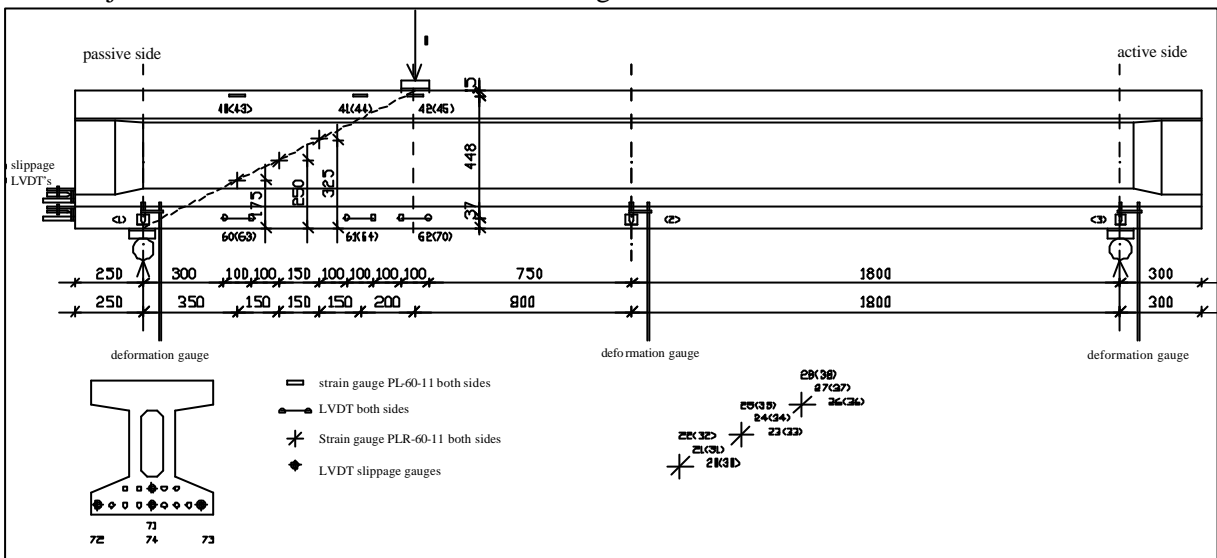


Figure 14 Measuring positions and devices for the shear test.

5.3 Measuring procedure for the torsion test

The lever arm is 1.5 metre. At the supports the torsional moment is transferred into two forces, acting on load cells. One positioned in the centre of the top flange depth and one at the centre of the bottom flange. Via the load cell the force is transferred to the steel frame, as shown in Figure 15. From the measured forces in the load cells, the acting torsional moment can be checked. Rollers are installed between the concrete flanges and the load cells to realise a free movement, rotation, of the flanges. Between the load cell and the concrete flange a steel plate 120 x 100 x 10 mm³ and 1 mm cardboard is applied to avoid a force transfer with peak stresses. The load cells are adjustable in length, so installed without any backlash.

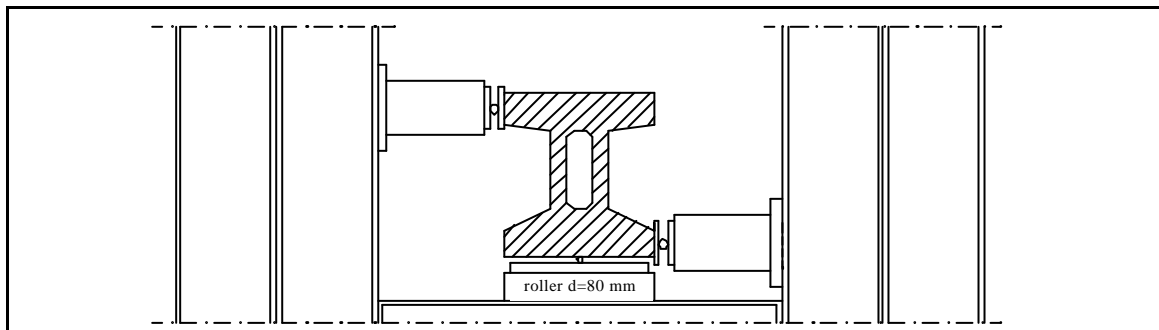


Figure 15 The fork-support for the torsion tests.

Under the beam a roller is installed, as for the shear tests, but now with the roller axis in longitudinal direction, to avoid an eccentricity in the vertical support reaction.

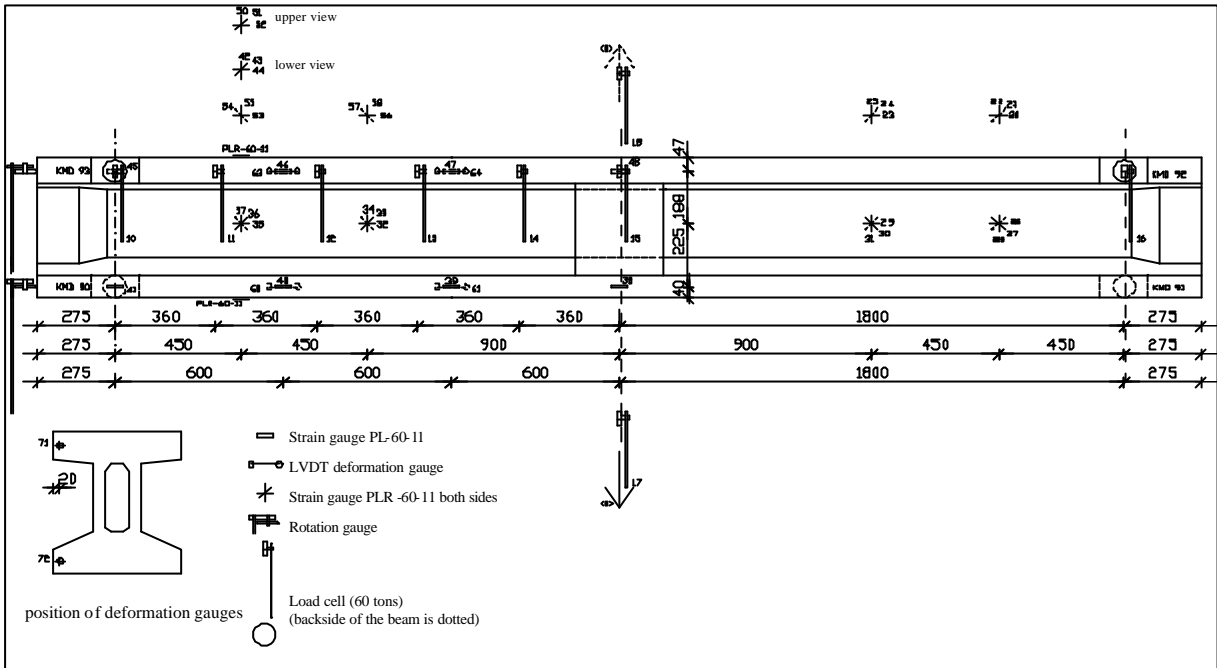


Figure 16 Measuring points and devices for the torsion test.

- The rotation of the beam is measured with rotation gauges, spread over half of the beam length, regarding the symmetry. From these rotations, the share of flange bending in the total acting torsional moment can be calculated or at least estimated.
- At both support rotation gauges to register any eventually rotation. Rotation gauges are also fixed to the jackets to indicate the rotation point of the beam.
- To measure the strains, due to flange bending, strain gauges are glued at the bending compressive side of the flange over half of the length of the beam. At the bending tensile side LVDT's are installed.
- To register an eventually clamped-in effect of the flange at the support side, strain gauges are glued in the centre of the support at the same side as the gauges installed to measure flange bending.
- Special strain gauges are positioned, measuring the strains in three directions. The principal stresses can be derived from the results. The measurements are performed on the webs at both sides of the beam, because it is not predictable whether the web fails at the left or the right side of the middle of the span.
- The gauges are also installed at the top and bottom side of the flanges. Due to the eccentrically prestressing of the beam, a clear difference in the principal stress direction must be visible.

- The rotation at the front of the beam is measured by 2 LVDT's positioned one above the other. At a certain load level the flanges tend to rotate in contrary direction.

In the first performed torsion test, the introduction of the load at the top of the flange was loading the flange itself too much, due to deformation of the steel beam in transverse direction, so the flanges showed a bending failure under the steel beam. In the next torsion test, the space between the flanges and the web has been filled up with concrete and coupled with anchors and steel plates.

5.4 Measuring procedure for the combined shear-torsion test

The drawing showing the measuring procedure is presented in Figure 17.

- The forces in the jackets to introduce the torsional moment are registered.
- The load cells at the support register the acting forces due to torsion.

Due to the introduced shear force in the test, a steel plate 100 x 120 mm² now replaces the roller under the beam at the support. A slight eccentricity in the support reaction is possible. There is no soft board present between the steel plate and the bottom side of the beam, because the load cells are not able to follow a vertical displacement of the beam as a whole.

- The rotation at several places along the beam is measured with rotation gauges.
- The rotation of the jacket that introduces the shear force is measured.
- Strain gauges and LVDT's are installed on the flanges, to estimate the share of flange bending in the torsion distribution.
- Special strain gauges are installed to measure the strains in 3 directions.
- The vertical displacement is measured at 1.0 m from the support.
- Strain gauges measure at the both sides the strain in the bending compression zone at 1.0 m from the support.

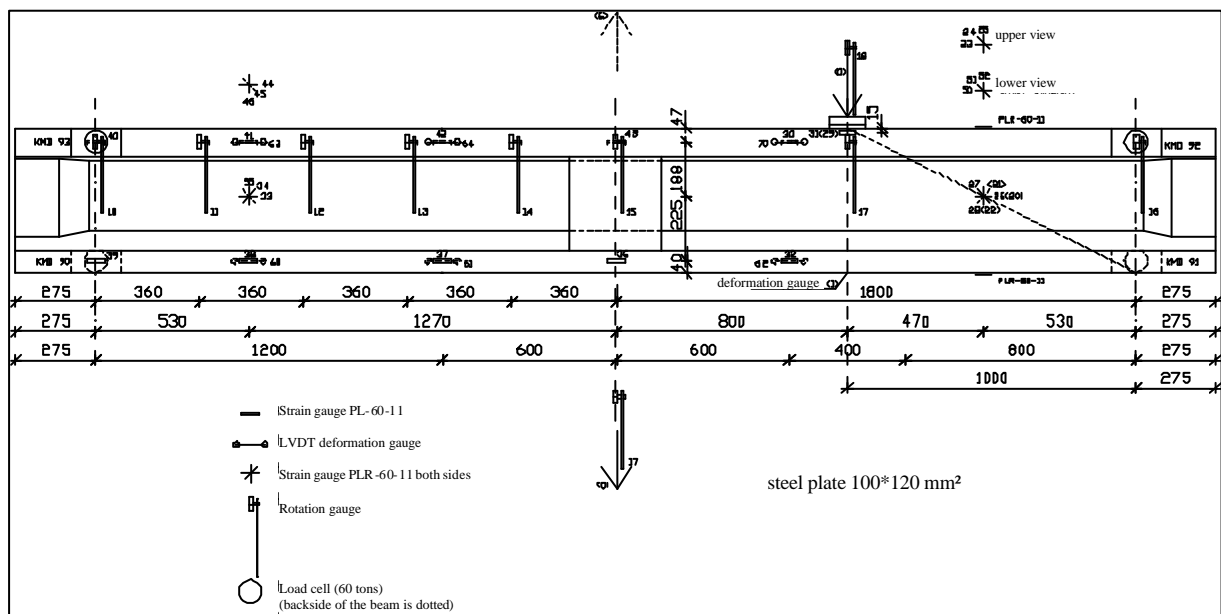


Figure 17 Measuring procedure for the shear- torsion test.

6 MEASURED RESULTS IN THE PRODUCTION STAGE

6.1 The measured transfer length of strands

6.1.1 The modification of the measuring procedure for some beams

The measuring procedure at prestress release is slightly modified after the first performed production. The modification is necessary when another production has to be prepared for the next day.

No modification was required for beams cast at Thursdays, because beams will never be cast on Friday. A complete measuring procedure is followed up for beam 1, 4, 8 and 12. The release of the prestressing force took about 20 minutes for the release in 5 steps.

For the other beams the prestressing force is slowly released in 1 step. The slippage, strain measurements and the camber measurements are then performed. The release of the prestressing force took approximately some minutes. The slippage of strand # 10 is measured with a digital sliding calipers. A complete data file can be found in [1].

6.1.2 The bond stress distribution along the strand

The real transmission of the released prestress force to the concrete is rather complex. The 'bond' stresses are distributed within the extremes showed in Figure 18.

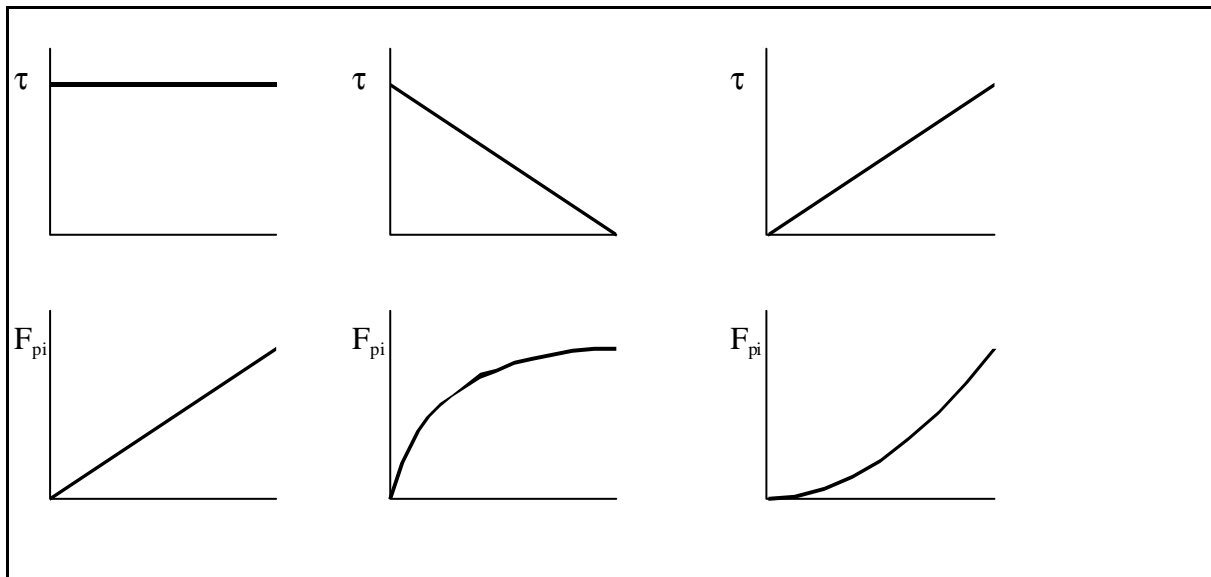


Figure 18 Bond stress distribution for released strands.

Within this research project the transfer length of the strands is equal to:

$$l_t = 1.35 \cdot l_{t,0.8} \quad (1)$$

In this formula:

$l_{t,0.8}$ is the distance in which 80% of the mean values of the maximum concrete strains are built up, according [5] and l_t = the transfer length of the strand.

A disadvantage of some methods to determine the transfer length of the strand is the presence and the use of local peak strains and has an empirical background. However, the applied method according [5] is based on mean values. Nevertheless, the transfer length is measured at the concrete surface, so in an indirect way.

An example is shown in Figure 19.

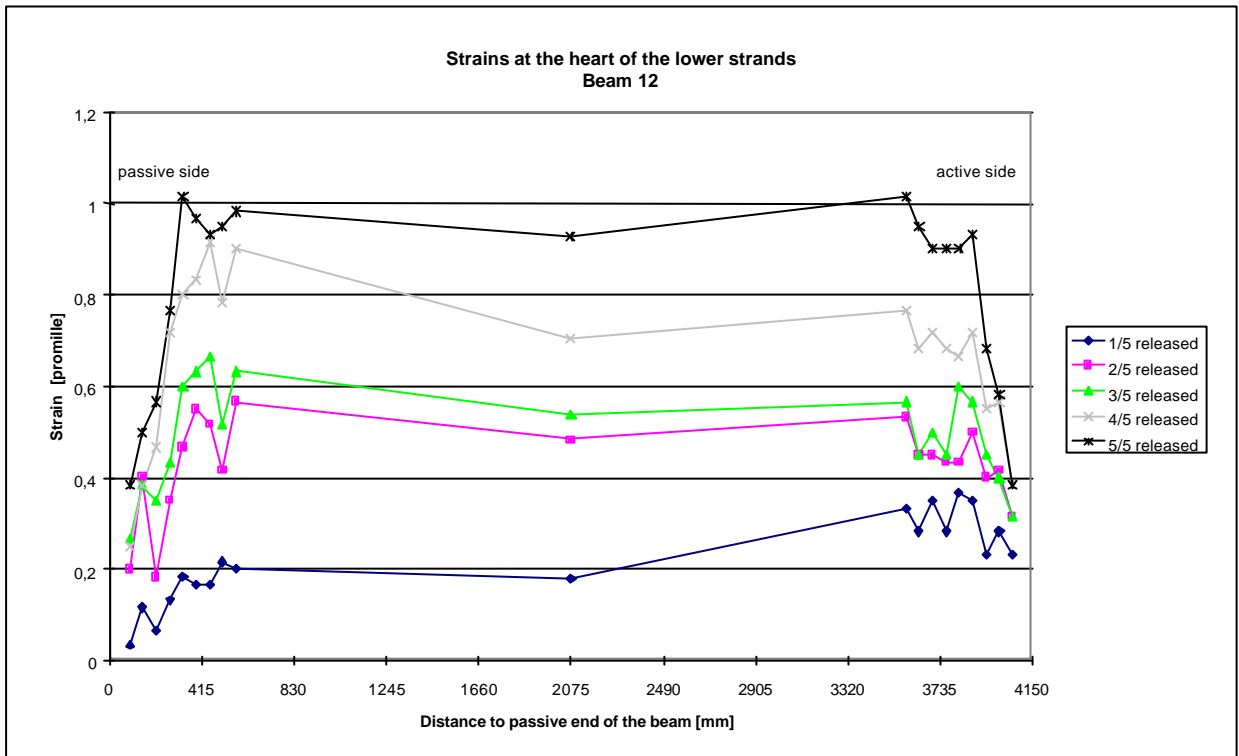


Figure 19 Measured deformations at the concrete surface.

From the measured slippage the bond distribution can be checked. The results of that are not always that satisfying, as desired.

6.1.3 Measured transfer lengths

The deformation of the concrete in the transfer zone of the released prestressing force is measured at the outside of the beam. In the mid section of the beam the deformations are more or less comparable in magnitude. According [5], the deformation at 80 % of the mean maximum deformation is determined as $l_{t,0.8}$. The transfer length $l_t = 1.35 \cdot l_{t,0.8}$.

In Table 5 the results are presented together with n, the number of steps at prestress release.

The transfer length is also calculated with the following formula, applying 10 for the value γ , according [5]:

$$l_{t,cal} = \gamma \cdot \sigma_k \cdot \sqrt{\frac{s_{pi}}{f'_{cm}}} \quad (1)$$

In the Dutch Code VBC 1995 and the CUR-Recommendation 37 for HSC, the following formula is given to calculate the design transfer length of a prestressing strand.

$$l_{o,VBC} = 0.5 \cdot \frac{\sqrt{f'_c}}{\sqrt{f'_{ck} = 39}} \cdot a_1 \cdot b \cdot \varnothing_k \cdot s_{pi} \cdot \sqrt{\frac{1}{f'_{ct}}}$$

for: $a_1 = 0.5$ and $b = 1$:

$$l_{o,VBC} = 0.04 \cdot \varnothing_k \cdot s_{pi} \cdot \sqrt{\frac{f'_c}{f'_{ct}}}$$

In fact, the transfer length is very depending on $\sqrt{f'_{ct}}$, which is a translation of the tensile stress. For HSC this result is not realistic enough. The values for f'_c and f'_{ct} can also be replaced by the mean values without making big mistakes. The formula is then as follows:

$$l_{o,VBC} = 0.04 \cdot \varnothing_k \cdot \sigma_{pi} \cdot \sqrt{\frac{f'_{cm}}{f'_{cmt}}}$$

For the mean compressive cube strength one can apply 115 N/mm². In Table 6.3.1 the calculated transfer length $l_{o,VBC 1995}$ is shown. Be aware that 10% deviation in f'_{ct} only results in 5% deviation in the calculated transfer length.

Table 5 Measured and calculated transfer lengths in mm.

N _{steps}	5	5	5	1	1	1	1	1	1	1	5	1
Beam	1	4	12	2	3	6	7	10	11	5*	8**	9***
σ_{pi}	981	1014	1136	1125	1019	943	1043	1040	1126	1078	1014	1106
f'_{cmt}	76	64	99	65	79	64	68	67	75	71	81	85
l_t active	260	308	331	557	331	377	437	572	437	708	257	663
l_t passive	305	345	361	437	256	512	422	572	542	542	343	361
$l_{t,cal} (?=10)$	464	513	437	537	463	495	505	509	500	503	456	466
$l_{o,VBC}$	623	701	632	771	634	651	700	704	718	707	623	664

Remarks:

- * Due to leakage of the jacket the prestress release for beam 5 was not performed correctly. The strands are cut at the active side, starting at the strand in the middle position. However, after having cut one strand, the force per strand increases. Around the strands small slivers of concrete peeled off. The relatively high values for the measured transfer length in beam 5 may be a result of the incorrect way the prestress release had to be performed.
- ** At the prestress release of beam 8, the jacket capacity was not high enough to release the wedges. Some strands are cut. There is no increase of the transfer length, however, studying the measured strains one may conclude that the high peak strains, at the active side in the first release steps, are a result of the way the prestress force is released.

*** In beam 9, in total 5 strands are cut, because the wedges could not be released. The transfer length at the active side increases substantially, due to the way the transfer length is determined from the measured deformation, say, strains. Another interpretation results in a transfer length of 377 mm.

As can be concluded from the measured transfer lengths, the one at the active side is not specifically longer than at the passive side. A stepwise release is advisable.

All measured transfer lengths are shorter than the calculated ones, as is logical. The transfer lengths in the Codes have to be conservative to cover the moment and shear capacity. However, a shorter transfer length increases the splitting tensile stresses!

For the following conclusions, the results of beams 5, 8 and 9 are neglected:

- The measured transfer lengths of beam 1, 4 and 12 are in the same range and all longer at the passive side. The prestress release is performed in 5 steps.
- Beams 2, 3, 6, 7, 10 and 11 do show more spread in the transfer lengths, which is more or less the same at the active as it is at the passive side.
- Although the conditions were not all the same, one may conclude, that the transfer lengths of the strands released in 5 steps is roughly 1.4 times shorter than when released in 1 step. This has to be studied separately once more. A stepwise release of the prestressing force is assumed in art. 9.7.3. of the VBC 1995/1995, while in the MC 90 a coefficient has to be taken in account, when not. The coefficient is 1.25.
- From the measured transfer lengths the value of λ_1 , as applied in formula (1) can be calculated and checked with the applied value $\lambda_1 = 10$. In
- Table 6 the results are presented as λ_1 .

Table 6 Value λ_1 , calculated from the measured transfer lengths

N_{steps}	5	5	5	1	1	1	1	1	1
Beam	1	4	12	2	3	6	7	10	11
s_{pi}	981	1014	1136	1125	1019	943	1043	1040	1126
f_{cmt}	76	64	99	65	79	64	68	67	75
$\lambda_{1 act}$	5.6	6.0	7.6	10.4	7.1	7.6	8.6	11.2	8.7
$\lambda_{1 pas}$	6.6	6.7	8.3	8.1	5.5	10.3	8.4	11.2	10.8

Results:

The mean value for beam 1,4 and 12 is: $\lambda_1 = 6.8$. The standard deviation 1.0

The mean value for beam 2,3,6,7,10 and 11 is: $\lambda_1 = 9.0$. The standard deviation 1.8

The value λ_1 is reviewed neglecting the influences of the active and passive side.

6.2 Slippage

As it is previously written, the slippage is measured for the beams 1, 4, 8 and 12 by using LVDT's at the active as well as at the passive side of the beams. However, the LVDT's are removed at the active side before the strands are cut, after the release step 5 is completed. No force was present anymore in the strands of beam 12 after release step 5.

The cut of the strands is registered at the passive side of the beams, except for beam 1, where a force of 16 kN was left in the bottom strands.

Using the measured slippage, the transfer lengths can be calculated with the following formula:

$$l_t = d_e \cdot a / e_{po} \quad (\text{in Table 6.2.1 presented as: } l_{t,de} \text{ act. and } l_{t,de} \text{ pas.})$$

The value for a is the one also implicitly applied in the formula $l_t = 1.35 \cdot l_{t,0.8}$.

Applied value for a = 2.345 [5].

Due to the wide spread of measured slippage values, in the next Table the mean values for the beams 1, 4, 8 and 12 presented. The slippage measured with a digital sliding calipers and the transfer lengths calculated from these, concern position 10 at the passive side of the beams 2, 3, 6, 10, 11 and 9.

The transfer lengths that are calculated from the measured slippage, according the formula (1) and the Dutch Code VBC, are also presented in Table 7.

Table 7 Transfer lengths calculated from the measured slippage [mm].

N _{ssteps}	5	5	5	1	1	1	1	1	1	1	5	1
Beam	1	4	12	2	3	6	7	10	11	5*	8**	9***
F _{po}	115	119	129	132	119	110	122	122	132	126	119	129
l _t act	260	308	331	557	331	377	437	572	437	708	257	663
d _e act	1.06	0.98	0.81	---	---	---	---	---	---	---	1.64	
l _{t,de} act	435 ⁺	388 ⁺	297	---	---	---	---	---	---	---	650	---
l _t pas	305	345	361	437	256	512	422	572	542	542	343	361
d _e pas	0.54	0.88	0.88	0.98	0.68	0.98	---	1.68	1.15	---	1.23	1.22
l _{t,de} pas	219 ⁺	348	321	348	268	419	---	648	409	---	486	406
l _{t,cal} (?=10)	464	513	437	537	463	495	505	509	500	503	456	466
l _{o,VBC}	623	701	632	771	634	651	700	704	718	707	623	664

+ The LVDT's are removed before the strands at the active side are cut.

The transfer lengths for beam 1 are increased with a factor $(1+16/114.7) = 1.14$, to eliminate the acting force of 16 kN. Then the results are:

$l_{i,de} \text{ act} = 496 \text{ mm}; l_{i,de} \text{ pas} = 250 \text{ mm}.$

For beam 4: $l_{i,de} \text{ act} = (1+23/118.6).388 = 463 \text{ mm}.$

- The measured slippage in beam 5,8 and 9 are neglected for reasons mentioned previously.
- The transfer lengths for beam 1 and 4 are longer now at the passive side than at the active side, just the opposite.
- The values for δ_1 can be checked, applying the transfer lengths based on the slippage measurements.

Table 8 The calculated values of δ_i .

N_{steps}	5	5	5	1	1	1	1	1	1
Beam	1	4	12	2	3	6	7	10	11
s_{pi}	981	1014	1136	1125	1019	943	1043	1040	1126
f_{cmt}	76	64	99	65	79	64	68	67	75
$\delta_1 \text{ act}$	5.6	6.0	7.6	10.4	7.1	7.6	8.6	11.2	8.7
$\delta_2 \text{ act}$	10.7	9.0	6.8	---	---	---	---	---	---
$\delta_1 \text{ pas}$	6.6	6.7	8.3	8.1	5.5	10.3	8.6	11.2	10.8
$\delta_2 \text{ pas}$	5.4	6.8	7.3	6.5	5.8	8.5	---	12.7	8.2

Conclusions:

The mean value of δ_i for beam 1, 4 and 12:

$\delta_1 = 6.8$ standard deviation = 1.0

$\delta_2 = 7.7$ standard deviation = 1.9

The mean value of δ_i for beam 2, 3, 6, 7, 10 and 11:

$\delta_1 = 9.0$ standard deviation = 1.8

$\delta_2 = 8.3$ standard deviation = 2.7 (exclusive beam 7)

The results of the active and passive sides are mixed.

Mutual differences are most likely related to a 5-step prestress release and a prestress release in one step, combine with strand cutting.

Without any further selection the average value for δ out of 29 is:

$\delta = 8.2$ standard deviation 2.0

When the results of research [5] is calculated the same way, from 26 data follows that:

$\delta = 8.1$ standard deviation 1.7

6.3 Splitting tensile stresses

Although the design calculation showed that the acting splitting tensile stresses were beyond the tensile capacity of the concrete, no cracks were visible after hardening. The hammer end as well as the additional stirrups must showed to be effective. Experience learns that the, also here, applied theory is a conservative one.

7 SHEAR FORCE CAPACITY OF THE BEAMS

The shear force capacity of three prestressed HSC beams is tested in a three-point bending test. The beam is provided with a high percentage of stirrup reinforcement to create a failure of the concrete strut. In the next part results of the tests are discussed. The belonging graph etc can be found in the Appendix.

7.1 Measured results analysed

7.1.1 Crack development

Monitored during the test:

- The first cracks appear in the webs. The inclination of the cracks is 25° to 30°, measured from the longitudinal axis of the beam.
- The crack development increases. Bending tensile cracks in the bottom flange appear at a force of 750 kN until 900 kN.
- The failure of the concrete strut is explosive, concrete is spalling from the web, the stirrups are visible.
- In the top flange some bending tensile cracks are visible, caused by the sudden failure of the concrete strut.
- In the web is temporarily a tensile force registered in the concrete strut directing, due to the dynamical effect caused by the failure. The upper flange shows then cracks. The strain gauges 40 and 343 tensile stress is registered.

Photographs are available in the Appendix, page 9 to 12.

7.1.2 Deflection

The deflecting of the beam during loading is measured in the middle of the span. The deflection of beam 3 is showed in Figure 20. There are four stages to observe:

1. Uncracked stage
2. First cracks in the webs; a small loss of stiffness.
3. Bending tensile stresses appear, cracks in webs develop further; stiffness decreases.
4. The cross-section is cracked, due to bending tensile stresses, visible easily; the stiffness decreases substantially.

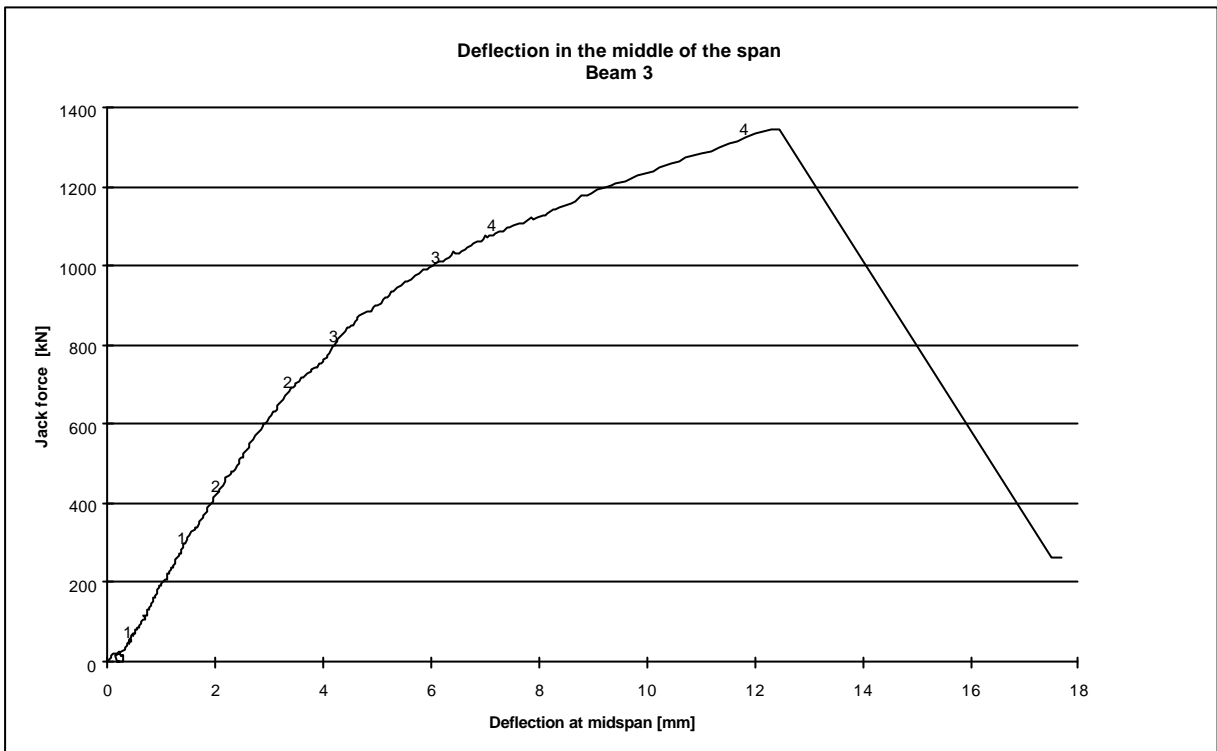


Figure 20 The measured deflection of beam 3 in the middle of the span.

The bending stiffness in uncracked stage is calculated with the E-modules measured at the test date.

The deflection and average stiffness are connected with each other via the following formula:

$$\delta_m = \frac{F \cdot a \cdot (3 \cdot l^2 - 4 \cdot a^2)}{48 \cdot E'_b \cdot I_b} \quad \rightarrow \quad E'_b \cdot I_b = \frac{F \cdot a \cdot (3 \cdot l^2 - 4 \cdot a^2)}{\delta_m \cdot 48}$$

Table 9 Mean bending stiffness of the beams during testing. [N/mm²].

Beam	1		2		3	
EI uncracked	1.74734.10 ¹⁴		1.73381.10 ¹⁴		1.82621.10 ¹⁴	
EI stage 1	1.72687.10 ¹⁴	98.8 %	-----*	-----*	1.82031.10 ¹⁴	99.7 %
EI stage 2	1.40392.10 ¹⁴	80.3 %	1.35978.10 ¹⁴	78.4 %	1.42820.10 ¹⁴	78.2 %
EI stage 4	3.71253.10 ¹³	21.2 %	3.91523.10 ¹³	22.6 %	3.94642.10 ¹³	21.6 %

* Not to determine for beam 2.

One may conclude that the calculated stiffness is close to the value measured in the test. Due to cracking in the web, the stiffness is reduced to 80% and when bending tensile cracks appear to 22 %, so substantially.

No slippage was noticed after the test, so the failure mode is not an anchorage failure.

7.1.3 Strains in the webs

The strains are measured in three directions by special strain gauges and are functioning as long as cracks pass the gauge. Elastic calculations, according the circle of Mohr, learn that the jacket forces necessary to exceed the principal tensile stress are in the range of 420 kN, 457 kN and 444 kN.

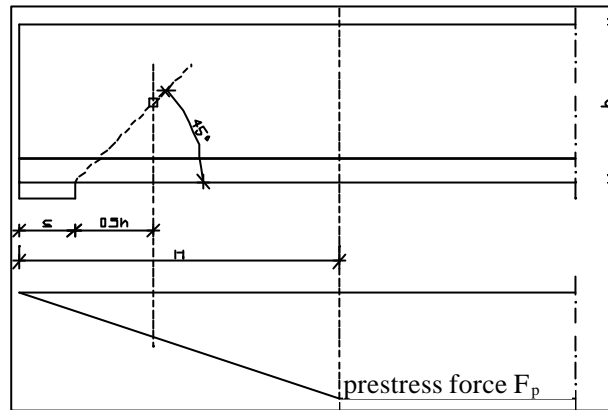


Figure 21 Cross-section in which the principal stresses are calculated.

However, the cracks do appear already at a lower load level. The possible reason might be that the mean value of the compressive stress, due to prestressing, as applied in the calculation, is not yet uniformly spread in the reviewed cross-section at 630 mm from the end of the beam, as shown in Figure 21.

There is no direct relationship between the inclination of the concrete struts and the inclination of the cracks.

By increasing the load the inclination of the concrete struts increases. The same trend is visible regarding the cracks. The upper limit is 40° .

In Figure 21 both the calculated and the measured inclinations of the concrete strut for beam 3 are presented.

The strain gauges of beam 2 and 3 were completely functioning until failure. The concrete strain at concrete strut failure is 2 ‰. This means, when taking in account a reduced value for the E-modulus, as measured and advised in [8], the ultimate compressive stress of the concrete strut is:

$$\text{Beam 2: } f_c^* \sim 0.002 \cdot 0.8 \cdot 39000 \sim 0.56 f_{cm}^*$$

$$\text{Beam 3: } f_c^* \sim 0.002 \cdot 0.8 \cdot 41350 \sim 0.53 f_{cm}^*$$

In which f_{cm}^* is the mean compressive cube strength.

The initial strain due to prestressing is not yet taken into account

7.1.4 Ultimate shear force capacity of the beams

The span of the beam in the test is 3.6 m. The force is introduced at 1.00 m from the support.

The shear force $V = F \cdot 2.6 / 3.6$

According the Dutch Code VBC 1995, a mean shear stress can be calculated as follows:

$$\tau_u = \frac{V_u}{b_w \cdot d}$$

In which,

b_w is the web thickness (2.45 = 90 mm)

d is the effective structural depth of the beam (500-60 = 440 mm)

The results of the tests are compared with the VBC 1995 and the CUR-Recommendation 37. Mean values are used to compensate long-term effects, when using short-term values.

$$\begin{aligned} \text{For } t_u = t_{2 \text{ CUR-37}} & \quad \text{instead of } t_2 = 0.1(f_c + 39) \cdot k_n \cdot k_\gamma & = & \quad 9.5 \cdot k_\gamma : \\ t_{2 \text{ CUR-37}}^* & = 0.1(0.85 \cdot f_{cm}(\text{beam}) + 0.85 \cdot f_{cm}(\text{C65})) \cdot k_n \cdot k_\gamma & = & \quad 9.5 \cdot k_\gamma \cdot ?_m / 0.85 \end{aligned}$$

In which:

0.85 the factor to modify the cube compressive strength into the uniaxial compressive strength.

$f_{cm}(\text{C65}) = 70 \text{ N/mm}^2$ (estimated mean cube strength)

$k_n = 1$

$k_\gamma = 1$ (for $\alpha = 90^\circ$)

$?_m = 1.27 = (0.72/0.68) \cdot 1.2$ so:

$$t_{2 \text{ CUR-37}}^* (\text{max.}) = 9.5 \cdot 1 \cdot 1.27 / 0.85 = 14.2 \text{ N/mm}^2$$

The results are presented in Table 10 as mean shear stress values:

Table 10 The measured and calculated values of t_u according CUR 37

Beam	1	2	3
f_{cm} [N/mm ²]	117.0	110.7	123.9
$F_{u \text{ jacket}}$ [kN]	1353	1283	1348
V_u [kN]	977	927	974
t_u [N/mm ²]	24.7	23.4	24.6
t_u [N/mm ²]	$0.21 \cdot f_{cm}$	$0.21 \cdot f_{cm}$	$0.20 \cdot f_{cm}$
$t_{2 \text{ CUR-37}}^*$ [N/mm ²]	14.2	14.2	14.2
$t_u / t_{2 \text{ CUR-37}}^*$	1.74	1.65	1.73

It is obvious that the additional safety margin is 1.6 to 1.7, when applying CUR 37.

When using the normal concrete Code VBC 1995 and choosing the same approach, the results are presented in Table 11.

Table 11 The measured and calculated values of t_u according VBC 1995

Beam	1	2	3
t_u [N/mm ²]	24.7	23.4	24.6
t_{2*VBC} [N/mm ²]	18.8	19.0	18.4
t_u / t_{2*VBC}	1.31	1.23	1.34

An additional safety margin of 1.2 or 1.3 is present.

However, it must be emphasised once more that the measured V_u is valid for the applied high stirrup reinforcement of $\pm 3.5\%$

The shear tests performed in DUT [3] are shown in Figure 22 together with the achieved shear test results at the EUT.

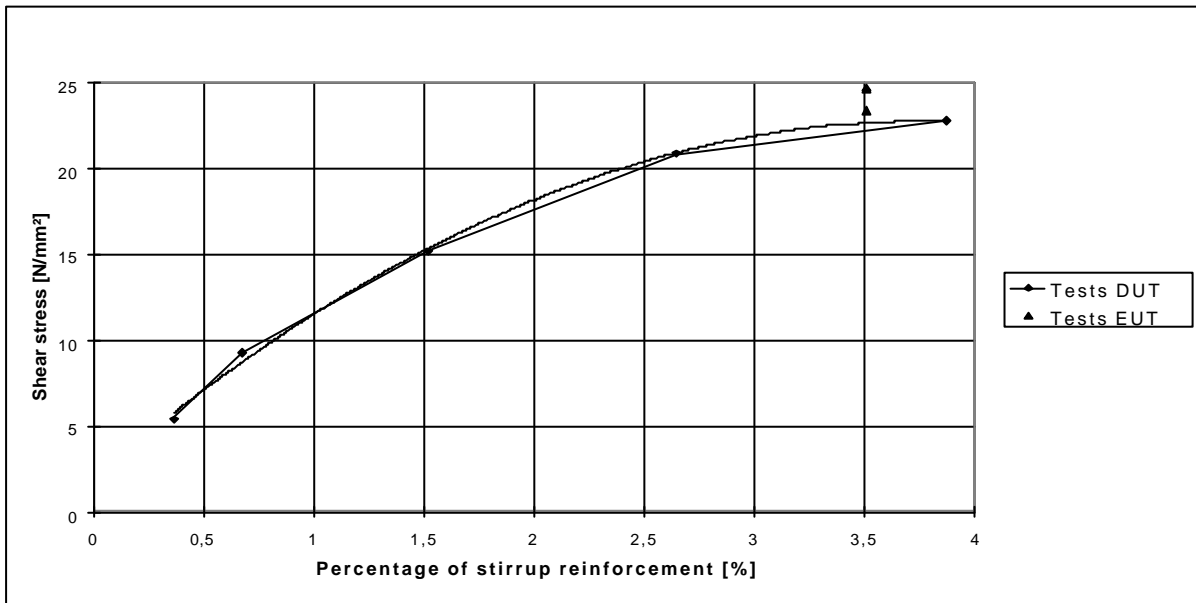


Figure 22 Comparison of the shear force test results DUT and EUT.

The results are very good comparable, especially when considering that the beams tested in Delft were non-prestressed ones.

Compared with the CEB-FIP Model Code 1990 and according the same approach:

$$f_{cd2} = 0.60 \cdot \left(1 - \frac{f_{ck}}{250}\right) \cdot f_{cd} \quad \rightarrow \quad f_{cm2} = \frac{0.60}{0.85} \cdot \left(1 - \frac{0.85 \cdot (f'_{cm})}{250}\right) \cdot 0.85 \cdot f'_{cm}$$

The shear capacity of prestressed beams

In which:

f_{ck} is the characteristic cylinder strength.

f_{cd} is the design value of the cylinder compressive strength.

f_{cm} is the mean compressive cube strength.

1/0.85 is the long-term factor

0.85 is the modification for cube strength into uniaxial compressive strength.

The shear force capacity is calculated with the following formula:

$$V_{u*MC90} = f_{cm2} \cdot b_w \cdot z \cdot \cos? \cdot \sin?$$

In which:

$$b_w = 2.45 = 90 \text{ mm}$$

$$z = 0.9 \cdot d = 0.9 \cdot 440 \sim 400 \text{ mm}$$

The obtained values are presented in Table 12, for the inclination $\theta = 30^\circ$ and 45° .

Table 12 Measured and calculated shear force capacity according MC 90.

Beam	1	2	3
V_u [KN]	977	927	974
V_{u*MC90} (30°) [KN]	659	646	671
V_u/V_{u*MC90} (30°)	1.48	1.43	1.45
V_{u*MC90} (45°) [KN]	761	746	774
V_u/V_{u*MC90} (45°)	1.28	1.24	1.26

The additional safety margin is for $\theta = 30^\circ$, 1.4 a 1.5.

For $\theta = 45^\circ$, 1.2 a 1.3

A final conclusion is:

Beams designed with a high stirrup percentage do have an additional safety margin:

1.71 when applying the CUR – Recommendations.

1.23 to 1.35 when applying the VBC 1995/1995

1.24 to 1.28 when applying the MC 90.

The CUR-Recommendation 37, regarding HSC, is too conservative concerning this aspect.

8 TORSIONAL CAPACITY OF THE PRESTRESSED BEAMS

The measuring and loading procedures are written previously in this Report. Three tests are performed with torsional moment acting in the middle of the span. The supports are fork type supports. The objective in the tests is to let fail the concrete struts, therefore a high percentage of stirrup reinforcement is applied. The results are discussed in the following parts. For graphs etc see the Appendix starting at page 22.

8.1 Measured results analysed

8.1.1 Crack development during the test

The photographs in Section 10.4 show the crack development of a beam during the test.

The following remarks can be made:

- At a torsional moment $T = 60$ kNm the first cracks are appearing in the webs of the beams. Next to that the first cracks in the front of the beam are visible.
- By an increasing torsional moment the crack development increases as well. Torsional cracks are also visible at the topside of the beam.
- At a torsional moment $T = 150$ kNm, cracks appear at the topside of the bottom flange. The cracks in the front increase substantially.
- Finally the web fails by shear at the ends of the beam. The partly separated webs like to move in opposite direction.

The aimed failure mode is not achieved.

8.1.2 The torsional moment checked

The load cells in the centre of the flanges do have a distance of $500-95/2-80/2 = 412$ mm.

The torsional moment acting at the support can be calculated. There is hardly any difference when checking T (applied) and T (support) at both sides of the beams.

- At $T = 200$ to 250 kNm differences between T (applied) and T (support) are noticed clearly. The torsional stiffness of the beam and parts of the beam change, due to cracking. The increase in one load cell means an equal decrease in the other one.
- The differences are more clear just before the beam fails, T (applied) differs from T (support). The deformations at the support do increase, friction as a result of that, may cause the differences.

8.1.3 Measured rotation

The rotation of the beam is measured with rotation gauges. For a higher torsional moment one finds a higher rotation. The measured rotation at point 15 differs from the one in point 14, although the values should be similar. The cross-section at the middle of the beam is made massive, see Figure 23.

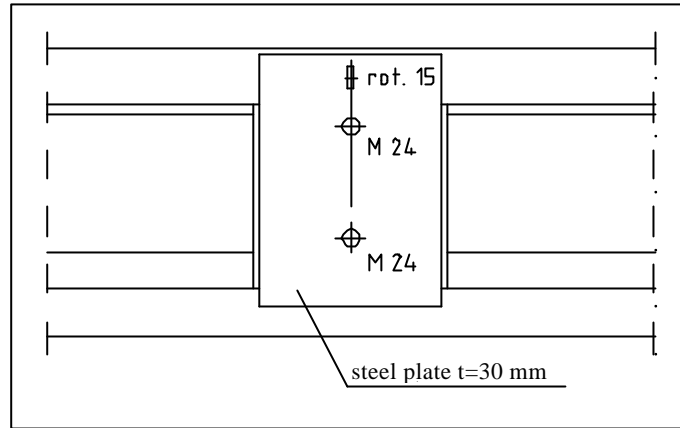


Figure 23 The front view of the beam in the middle of the span.

In Table 13 the mean torsional stiffness of the beam is presented for the first stage of the loading, $T = 50$ kNm as well as for the last 50 kNm before failure.

Table 13 The mean torsional stiffness during the tests [Nmm²].

	Beam 5	Beam 6	Beam 7
$GI_{wr} 0-50$	$52.3 \cdot 10^{12}$	$62.5 \cdot 10^{12}$	$71.4 \cdot 10^{12}$
$GI_{wr} (Tu-50) - Tu$	$6.0 \cdot 10^{12}$	$3.3 \cdot 10^{12}$	$5.3 \cdot 10^{12}$
$GI_{wr} 0-50 / GI_{wr} (Tu-50) - Tu$	8.7	19.2	13.5

The decrease in stiffness is substantially as soon as the beam shows cracks..

The rate of flange bending can be analysed more easily, when the rotation along the beam is printed and the connecting conditions are reviewed. A certain influence of a moment at the support, due to the cantilevered part of the beam is present. When cracks appear in the cantilevered part, the influence of the support decreases. The support can be seen as a fork support. The rotation in the middle of the beam is not the highest one.

8.1.4 Measured strains

The strain gauges are glued at the bending compressive zone of the flanges and register an increasing strain at an increase of the torsional moment. The measured strains at the top flange are higher than at the bottom flange. This may be caused by the eccentricity of the prestressing force. Cracks at the top flange do lower the centre of gravity in the cross-section.

Studying the measured strains and displacements, an indication can be found concerning the magnitude of the flange moment. Compared with the calculated flange moments, the measured ones are lower. But in the flanges there is torsion acting next to flange bending.

In Figure 24 the results of measurements and theoretical approaches are showed.

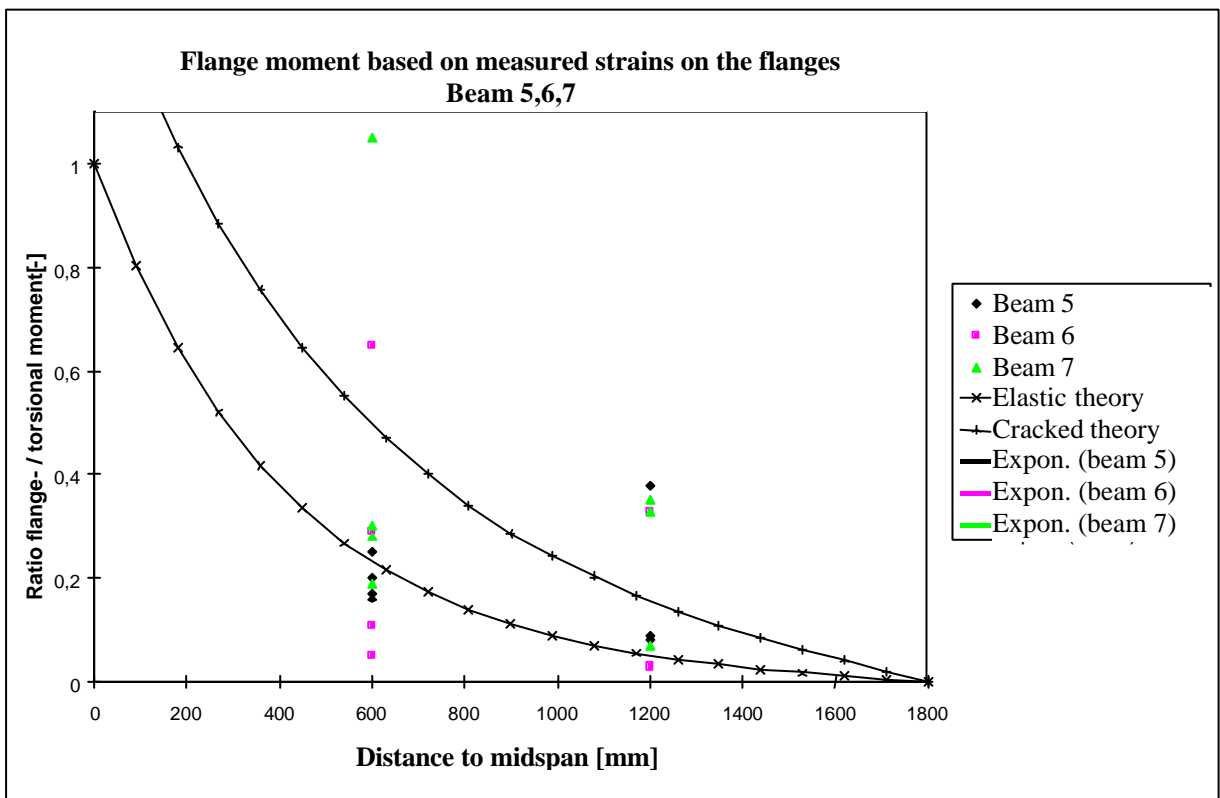
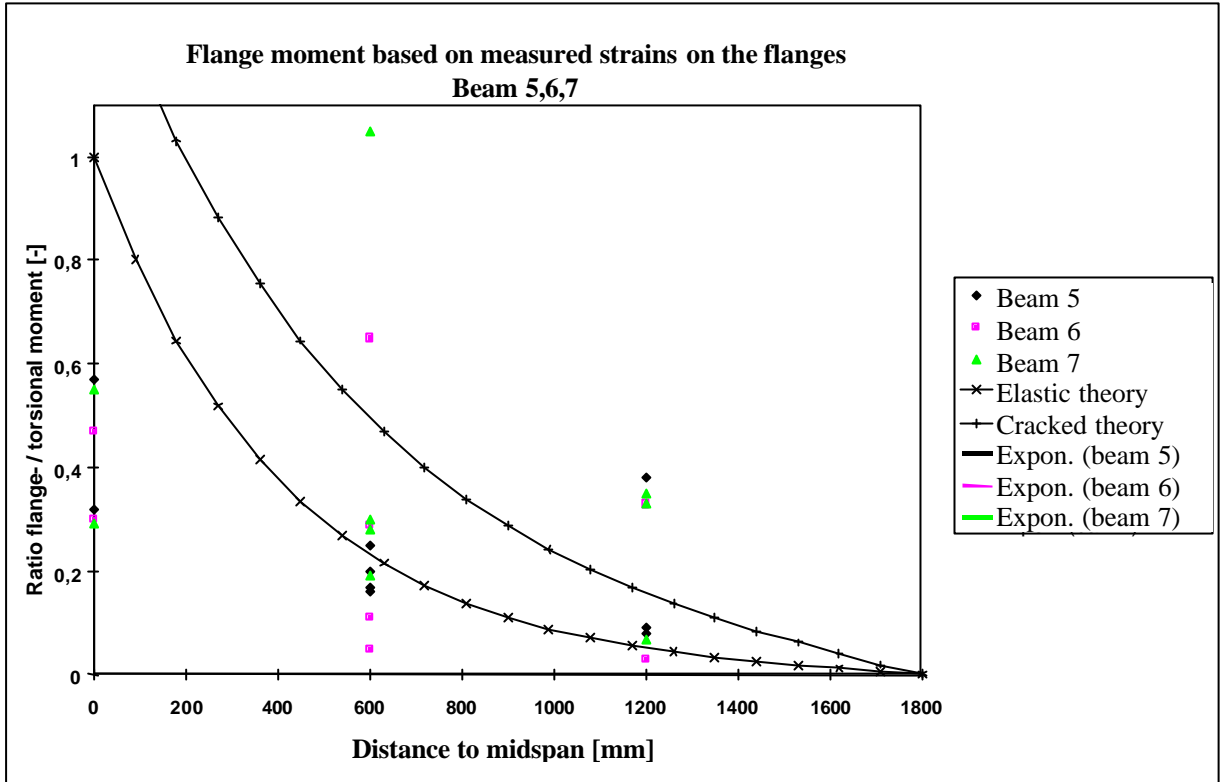


Figure 24 Flange moment calculated from measured strains.
 A. The stiffness of the massive part in the middle of the beam is not taken into account.
 B. The additional stiffness is taken into account.

The angle of the compression and tensile stresses do change, due to cracking. Cracks appear in the web under an angle of 30°; the upper limit is 40°. The bottom flange does crack in a later loading stage. Cracks in the top flange appear under an angle of 45° or 50°.

8.1.5 The torsional capacity of the beam

According VBC 1995, article 8.4, the torsional capacity can be calculated as follows:

$$\tau_d = \frac{T_{di}}{W_t} \leq \tau_s = t_2$$

In which:

- t_d is the design shear stress
- t_s is the design stress due to reinforcement
- t_2 is the design stress, due to the ultimate concrete strut capacity.
- T_{di} is the torsional moment in the f - rectangular part of the cross-section
- W_t is the section modulus for torsion of the reviewed rectangular sub-section

The capacity of the concrete strut is essential, due to the high rate of applied stirrup reinforcement. In CUR – Recommendation 37 the value $t_2 = 7 \text{ N/mm}^2$. Taking in account the mean values for the concrete strength instead of characteristic ones, the long-term effects are compensated.

The modification of t_2 is as follows: $t_{2,CUR}^* = 7 \cdot 1.27 / 0.85 = 10.46 \text{ N/mm}^2$.

The section modulus for torsion is known, when one assumes flange dimensions (95 x 450 mm) and for the outside dimensions of the web (170 x 500 mm).

$$T_{u,CUR} = 2 \cdot (2 \cdot t_{2,CUR}^* \cdot W_{t,flange} + t_{2,CUR}^* \cdot W_{t,web}) = 2 \cdot (2 \cdot 10.46 \cdot 1201552 + 10.46 \cdot 4000514) \cdot 10^{-6} = 134 \text{ kNm}$$

The calculated T_u can be compared with the measured ones, see Table 14.

Table 14 Measured and calculated torsional moments compared.

	Beam 5	Beam 6	Beam 7
T_u	268	281	240
$T_{u,CUR}$	134	134	134
$T_u / T_{u,CUR}$	2.00	2.10	1.79

An additional safety factor of 1.8 and higher is left, when calculating according CUR-Recommendation 37. However in the calculation, according the VBC 1995, flange bending is not reviewed. The influence of flange bending is important. Just before failure $\pm 25\%$. Nevertheless the additional safety margin modified with 25% is still high.

The concrete strut did not fail as expected. In fact, the capacity of the concrete strut is not fully explored, so the additional safety factor increases.

9 SHEAR AND TORSIONAL CAPACITY OF BEAMS

After loading the beams with 25, 50 or 75% of the torsional moment T_u , as measured in previous tests, the shear force is introduced until failure, while the torsional moment does not change.

The shear force is applied at the very moment the beam has been deformed by the torsional moment. This sequence avoids that the already applied shear force has to follow the rotation of the beam under torsion.

The objective is again to let fail the concrete strut in the webs. The test arrangements are the same as applied for the shear force test and the torsion test. The location for the introduction of the jacket forces is similar to the ones for the individual tests on shear or torsion.

The results of the tests are discussed in the next part. The graphs and photos are found in the Appendix starting at page 42.

9.1 Measured results analysed

9.1.1 Crack development during the test

A torsional moment is introduced in the middle of the span of the beam. The introduced torsional moment is respectively 65, 130 or 195 kNm, which is 25%, 50% and 75% of T_u , measured in the series torsion tests.

The following aspects are noticed:

- At $T = 65$ kNm, small cracks are visible in the webs.
- At $T = 130$ kNm, the webs are cracked.
- At $T = 195$ kNm, the cross-section is cracked, included the (prestressed) bottom flange.

The shear force is then introduced.

- More cracks appear, especially in the direction where the shear stresses, due to shear force and torsional moment, are acting in the same direction.
- The inclination, the angle of the cracks, is more or less the same.
- At the other side of the beam new cracks do appear only after $V = 600$ to 750 kN, because the cracks, due to torsion and shear, are working in opposite directions.
- By increasing the load, bending tensile cracks appear in the bottom flange of the beam.
- For the beam with $T = 65$ kNm, the failure is explosive, both sides of the beam fail almost at the same very moment.
- For the beams with $T = 130$ kNm, respectively 195 kNm, the concrete strut in the web fails. The web fails at the side of the beam where stresses, due to shear and torsion, act in the same direction. The concrete strut failure in the web is explosive; the concrete cover is spalling.

9.1.2 The torsional moment checked

The torsional moment, calculated from the registered forces in the load cells, is almost the same as the introduced one. The small differences are caused by the replacement of the roller by the steel plate underneath the beam. A free rotation is therefor slightly hindered.

The differences in introduced and registered moment are increasing by an increase of V . The reaction force in point 92 is decreasing, due to the slightly hindered rotation at the bottom side of the support. The reaction force at the other side increases. The difference between the two reaction forces is the friction force in the steel support of the jacket, as shown in Figure 25.

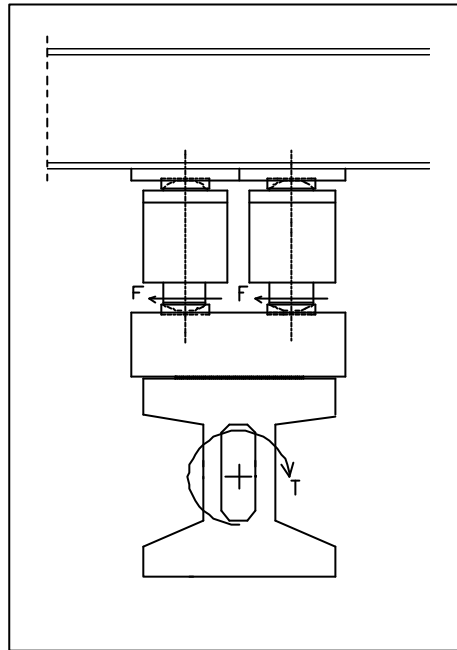


Figure 25 Friction forces in the socket of the two jackets.

9.1.3 Measured rotation

Rotation gauges measure the rotation of the beam. The rotation measured at position 15 is less than measured for point 14. A small disturbs in the curve means probably the appearance of another crack.

In the graph, shown in Figure 26, the applied torsional moment is clearly visible. An increase of V causes more cracks and so, the decrease of the torsional stiffness.

9.1.4 Measured strains

The strains are comparable with the strains measured in the torsion tests, until the shear force is introduced. The strains, measured close to the shear force jackets, increase most of all. The beam is already cracked before the shear force is introduced. Strain gauge 31 shows a change of sign.

The increase of the strain is comparable with the increase of strain in previous tests.

The differences in bending stiffness of the beams are small. Beam 11, loaded with $T = 65$ kNm shows to be stiffer than the other ones. However, the bending stiffness of the tested beams is substantially decreased. The deflections, measured during the 5 tests are shown in Figure 26.

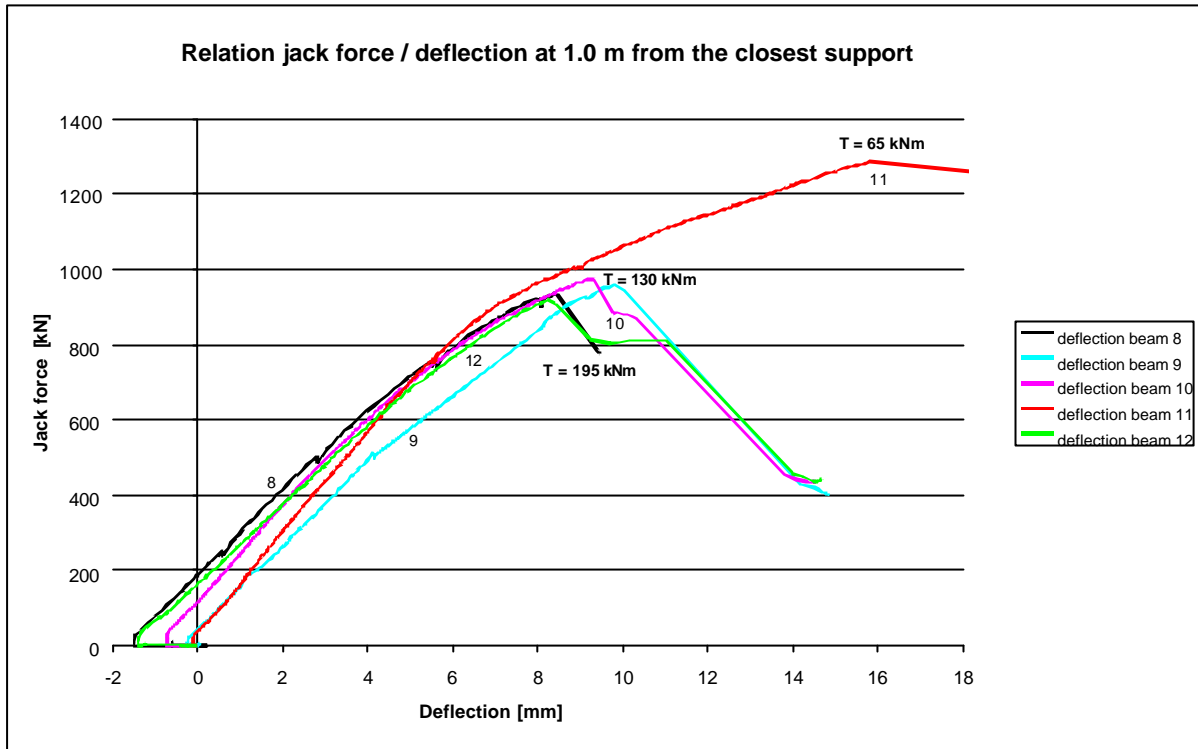


Figure 26 Measured deflections at 1.0 m from the closest support.

The principal directions of the concrete strut are comparable with those measured and calculated in the torsion test. By an increase of the shear force V the angle of the concrete strut in the top flange decrease, while in the bottom flange the angle increases.

9.1.5 Flange bending and torsion

The ratio of flange bending in the total applied torsional moment can be calculated, following the basic elastic theory [1]. The support functions as a fork support, as can be read from the measured data. Therefore it is possible to calculate the same rotations as measured, by iteration.

The calculation are made at the positions of the rotation gauges 11, 12, 13 and 14 and for a torsional moment of 25, 50, 75 and 85% of the mean value of T_u , that is the mean torsional capacity of beam 5,6 and 7.

The location of the rotation gauges is shown in Figure 27.

- $T_{u\text{ mean}} = 263 \text{ kNm}$
- 25% ? $T = 65 \text{ kNm}$
- 50% ? $T = 130 \text{ kNm}$
- 75% ? $T = 195 \text{ kNm}$
- 85% ? $T = 225 \text{ kNm}$

It is assumed that the ratio flange bending and torsion of the box girder is known when the measured and the calculated rotations fit. The middle section is partly massive and therefore neglected in the calculations.

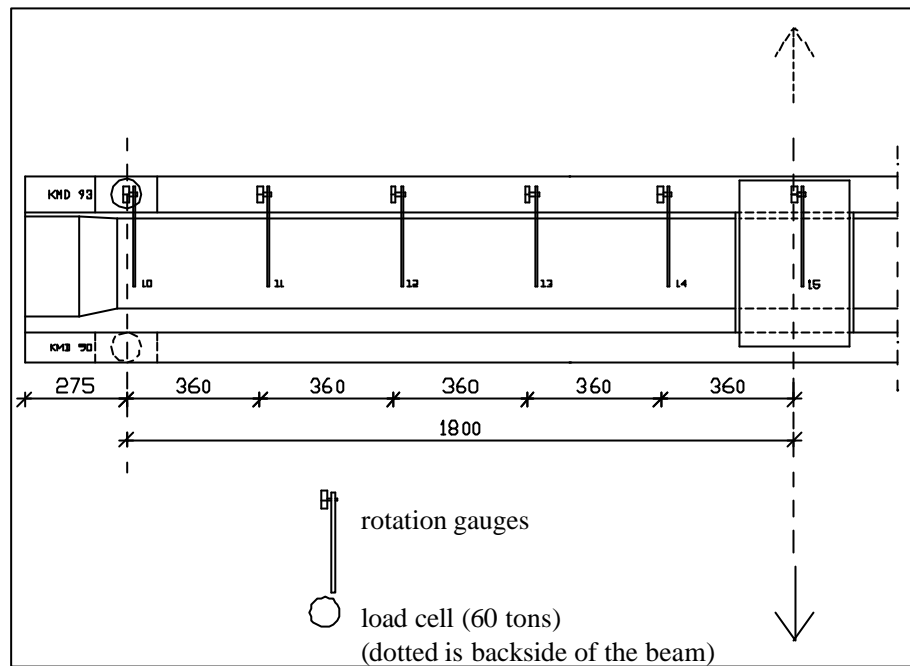


Figure 27 Location of the rotation gauges.

The calculation results are shown in Figure 28 to Figure 31 for the rotation gauges 11 until 14.

- The location of rotation gauge 11 is at 360 mm from the support. It is decided not to try to find any regression function.
- Rotation gauge 12 shows that by an increase of the torsional moment the share of flange bending is increasing and torsion in the box girder is decreasing.
- Rotation gauge 13 shows that the share of flange bending is higher than at location 12 and almost 50% of the introduced torsional moment, just before failure of the beam.
- Rotation gauge 14 shows the trend of the increase of flange bending as share of the introduced torsional moment.

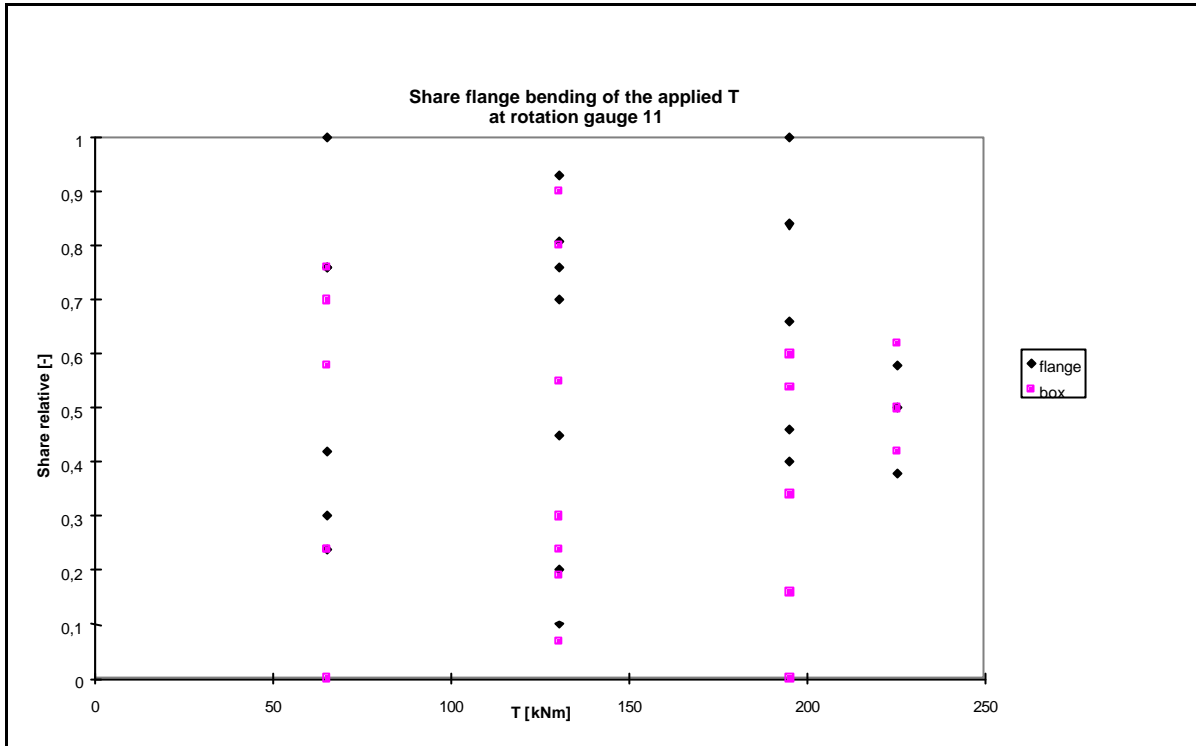


Figure 28 Rotation gauge 11- share flange bending of the applied T

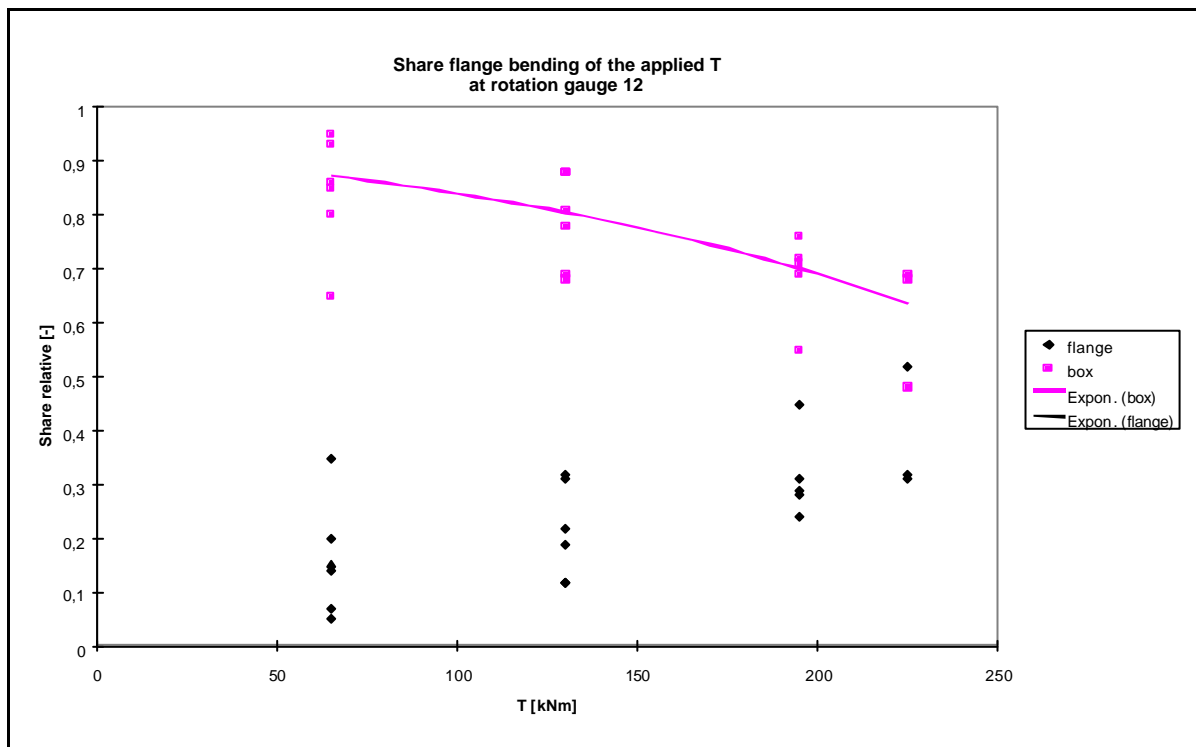


Figure 29 Rotation gauge 12- share flange bending of the applied T.

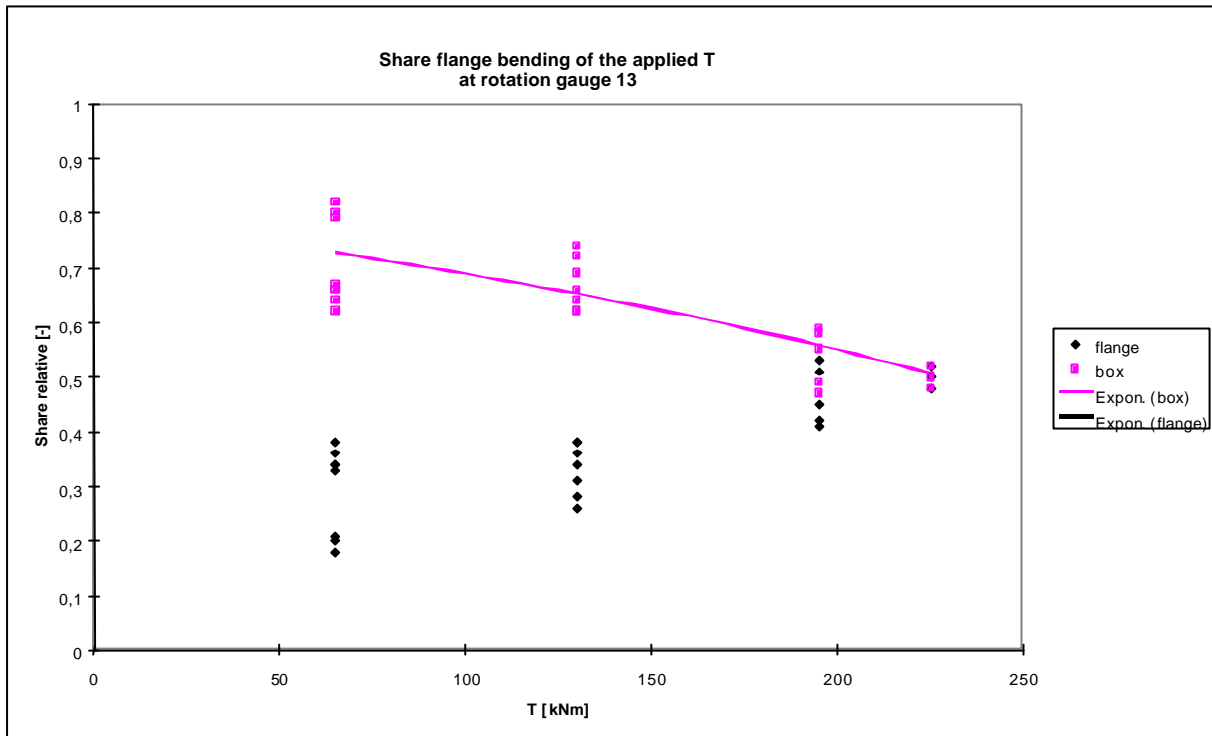


Figure 30 Rotation gauge 13- share flange bending of the applied T

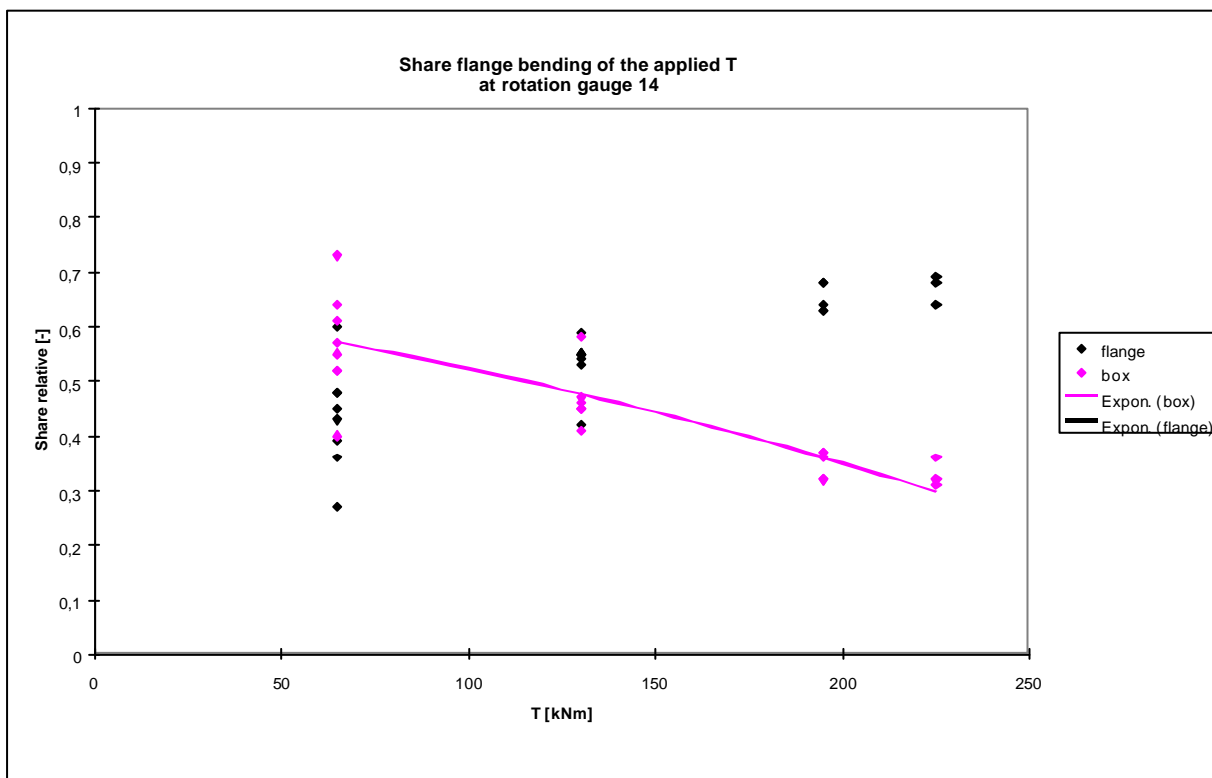


Figure 31 Rotation gauge 14- share flange bending of the applied T

In Figure 31, the share of flange bending of the total introduced torsional moment T is presented along the axis of the beam. The tendency is clear. The flange bending increases with an increase of the torsional moment, while the torsion of the box girder at the same time decreases.

In the same Figure the dotted line 5 shows the share of flange bending according the theoretical model. The dotted line 6 shows the results for a cracked cross-section.

It is obvious that the share of flange bending increases because the torsional stiffness decreases, due to the crack development during the test. The showed results can be used, to calculate the torsional moment causing shear stresses in the webs and in the flanges. One has to separate the torsional moment acting in the flanges and in the box girder.

9.1.6 The ultimate capacity of the beam

The ultimate capacities for the designed beam can be calculated according the Dutch concrete Code VBC 1995, article 8.5. The short-term mean value $t_{2\text{CUR}}^* = 7 \cdot 1.27/0.85 = 10.46 \text{ N/mm}^2$

From the measured results, the ultimate shear stresses can be calculated according the following formulas:

$$\tau_T = \frac{T_{\text{koknetto}}}{2 \cdot 125 \cdot b_1 \cdot d} \quad \tau_V = \frac{V_u}{b_2 \cdot d}$$

In which:

- 2 The shear flow is constant, so the webs and flanges do have the same share
 125 c.o.c. distance of the webs [mm]
 $b_1 =$ 45 mm (web thickness)
 $b_2 =$ 90 mm (thickness for two webs)
 $d =$ 440 mm (effective structural beam depth)

The results of the calculations are presented in Table 15.

Table 15 Comparison of the measured ultimate capacity and the calculated one, according CUR-Recommendation 37, for shear force and torsional moment.

Beam	8	9	10	11	12
T/2	97.5	65	65	32.5	97.5
$T_{\text{box total}}$	67.28	53.95	53.95	28.28	67.28
$T_{\text{box netto}} (0.733)$	49.32	39.55	39.55	20.73	49.32
t_T	10.0	8.0	8.0	4.2	10.0
V_u	676	694	698	928	663
t_V	17.1	17.5	17.6	23.4	16.7
$t_T + t_V$	27.1	25.5	25.6	27.6	26.7
$t_{2\text{CUR}}^*$	10.5	10.5	10.5	10.5	10.5
$(t_T + t_V) / t_{2\text{CUR}}^*$	2.58	2.43	2.44	2.63	2.54

The additional safety margin is ± 2.5 before the beam fails.

The same is done when applying the Dutch Concrete Code VBC 1995.

$$t^*_{2 \text{ VBC 1995}} = 0.2 \cdot 0.85 \cdot f'_{cm} \cdot k_n$$

The results are presented in Table 16.

Table 16 Comparison of the measured ultimate capacity and the calculated one, according the Dutch Concrete Code VBC 1995, for shear force and torsional moment.

Beam	8	9	10	11	12
T/2	97.5	65	65	32.5	97.5
T _{box total}	67.28	53.95	53.95	28.28	67.28
T _{box netto} (0.733)	49.32	39.55	39.55	20.73	49.32
t _T	10.0	8.0	8.0	4.2	10.0
V _u	676	694	698	928	663
t _V	17.1	17.5	17.6	23.4	16.7
t _T + t _V	27.1	25.5	25.6	27.6	26.7
f'_{cm}	130.3	119.2	128.0	127.5	126.6
t^*_{2}	22.2	20.3	21.8	21.7	21.5
(t _T + t _V) / t^*_{2 \text{ VBC}}	1.22	1.26	1.17	1.27	1.24

The additional safety margin is 1.23. This comparison is only valid for the applied 3.5% stirrup reinforcement.

The same is now calculated according the MC 90.

Due to torsion, the concrete stress in the concrete strut is:

$$V_T = \frac{T_{box,netto} \cdot z_i}{2 \cdot A_{ef} \cdot d} \Rightarrow f'_{cT} = \frac{V_T}{t_i \cdot z_i \cdot \cos \mathbf{q} \cdot \sin \mathbf{q}}$$

Due to shear force, the concrete stress in the concrete strut is:

$$f'_{cV} = \frac{V_u}{b_w \cdot z \cdot \cos \mathbf{q} \cdot \sin \mathbf{q}}$$

In which:

- z_i is the distance c.o.c. of the equivalent flange; 436.6 mm
- A_{ef} is the surface within the centre lines of the parts; 125. 436.6 mm²
- d is a factor for the cross-section ; 1-0.25b/h
- t_i is the web thickness; 45 mm
- q is the inclination of the concrete strut, here 30°.
- b_w is the total web thickness for the cross-section; 90 mm
- z is the lever arm = 0.9.d

Table 17 Calculation of ultimate capacity of the concrete strut measured and calculated, according the Model Code 1990, due to shear force and torsional moment.

Beam	8	9	10	11	12
T/2	97.5	65	65	32.5	97.5
T _{box total}	67.28	53.95	53.95	28.28	67.28
T _{box.netto} (0.733)	49.32	39.55	39.55	20.73	49.32
f _{cT}	25.2	20.2	20.2	10.6	25.2
V _u	676	694	698	928	663
f _{cV}	43.8	45.0	45.2	60.1	43.0
f _{cT} + f _{cV}	69.0	65.2	65.4	70.7	68.2
f _{cm}	130.3	119.2	128.0	127.5	126.6
(f _{cT} +f _{cV})/f _{cm}	0.53	0.55	0.51	0.55	0.54

The relative ultimate compressive stress of the concrete strut is $> 0.51 \cdot f'_c$, in which f'_c is the mean compressive cube strength for cubes $100 \times 100 \times 100 \text{ mm}^3$.

The reduction of the compressive strength in the concrete strut is caused by the acting tensile stresses in the stirrups.

The ultimate compressive stress of the concrete strut for the performed shear tests of beam 1,2 and 3, is presented in Table 18.

Table 18 Calculation of ultimate capacity of the concrete strut measured and calculated, according the Model Code 1990, due to shear force.

Beam	1	2	3
V _u	977	927	974
f _{cV}	63.1	60.0	63.3
f _{cm}	117.0	110.7	123.9
f _{cV} /f _{cm}	0.54	0.54	0.51

The relative ultimate compressive stress of the concrete strut is $> 0.51 \cdot f'_c$, in which f'_c is the mean compressive cube strength for cubes $100 \times 100 \times 100 \text{ mm}^3$. This is the same as for the tests for shear force and torsional moment.

However, the failure load is now slightly lower. The beams, applied for the shear force and torsional moment capacity, are 180 days older of age. The mean cube strength is 11% higher.

In the torsion test itself, the ultimate capacity was not achieved.

Conclusion:

In fact, the failure load for the concrete strut is the same for shear force as for shear force and torsional moment. It is possible to present the failure envelope, due to shear force and torsional moment, valid for the prestressed HSC beam with 3.5% stirrup reinforcement.

The shear capacity of prestressed beams

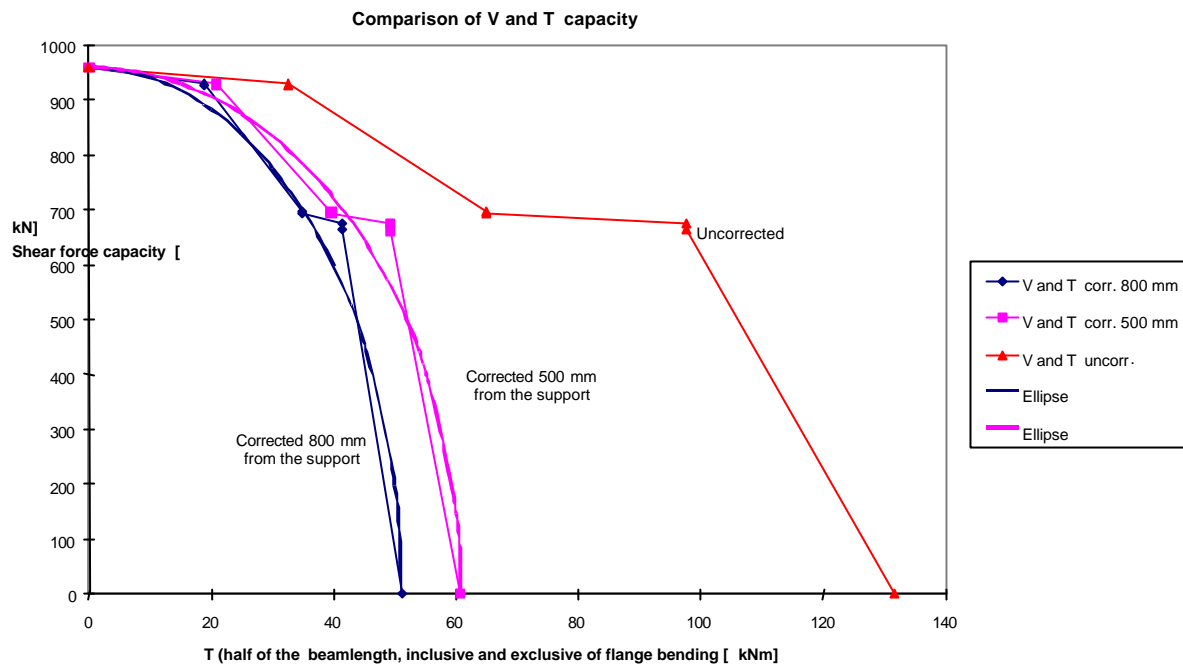


Figure 32 Failure envelop, due to torsional moment and shear force.

10 PRESTRESSED LWA CONCRETE BEAMS

10.1 A new cross-section

The behaviour of the HSC beam is rather complicated and not easy to describe, as explained in the previous chapters. Therefore it has been decided finally to modify the cross-section of test beam for the second series. The cross-section is a box.

The conditions for the modification are as follows:

- The cross-sectional area A , identical.
- The second moment of area I , identical
- The length will not change

These conditions are fulfilled in the new cross-section almost completely. For production reasons mainly, the web thickness is 50 mm instead of 45 mm. The flanges are 105 mm deep.

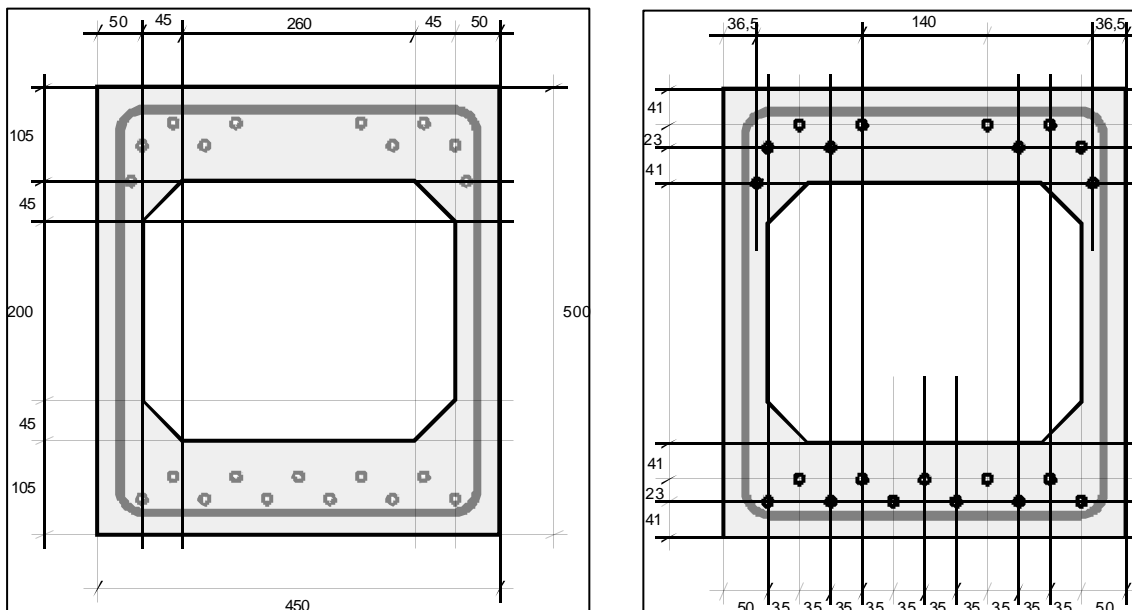


Figure 33 Cross-section of the beam

The objective is again to let fail the compressive concrete strut.

The bottom flange of the beam is prestressed with 11 strands ϕ 12.9 mm, $A_p = 100 \text{ mm}^2$. However, prestressed at 1100 N/mm^2 , lower initial stress than in the previous series. The top flange of the box beam is prestressed with 10 strands ϕ 12.9 mm, $A_p = 100 \text{ mm}^2$, FeP 1860. The initial stress in the strands is 200 N/mm^2 .

The stirrups are designed with the knowledge gained in the first test series. The stirrup reinforcement is ϕ 10-75 mm, FeB 500 or S500. At the end of the beam 3 extra stirrups are applied to avoid crack propagation.

10.2 The production of the beam

The beam is produced by Hurks Beton B.V. for the same reasons as in the first stage of the project., too much projects at the same time and a too low concrete mixer capacity.

The mix design is rather identical to previous tests with LWAC. The mass is 1950 kg/m³.

Table 19 Mix composition

Constituent materials per 1000 litre.	Weight [kg]
Sand 0-4	585
Lytag 4-12	720
Cement Anneliese CEM I 52.5 R	375
Water (w.c.r. = 0.40)	150
Calcitec Limestone powder	25
Superplasticizer OFT III	2.63
Superplasticizer ON 2	1.88

Some photos show the stages of the production of the beams:



Figure 34 Stirrup reinforcement

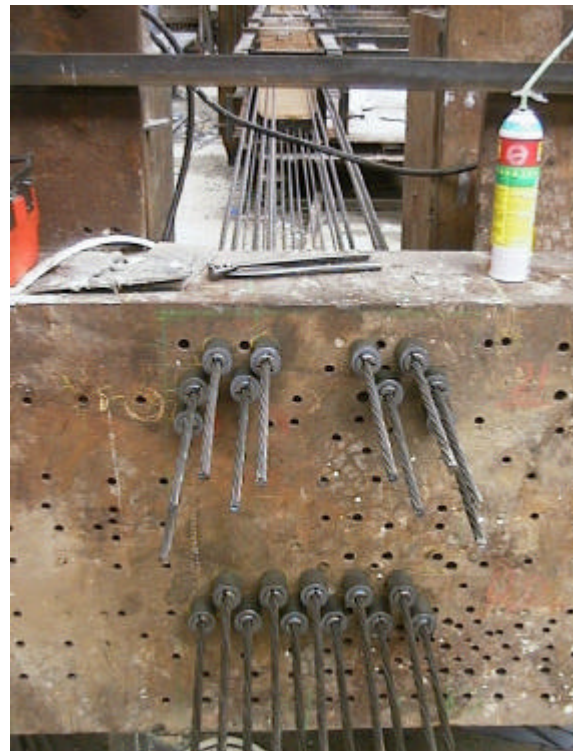


Figure 35 End zone of the beam



Figure 36 End zone of the beam and prestress strands

10.3 The test arrangements

Due to the modified cross-section the torsional moment will now be introduced at the end of the beam. The test arrangements are shown in the next Figures.

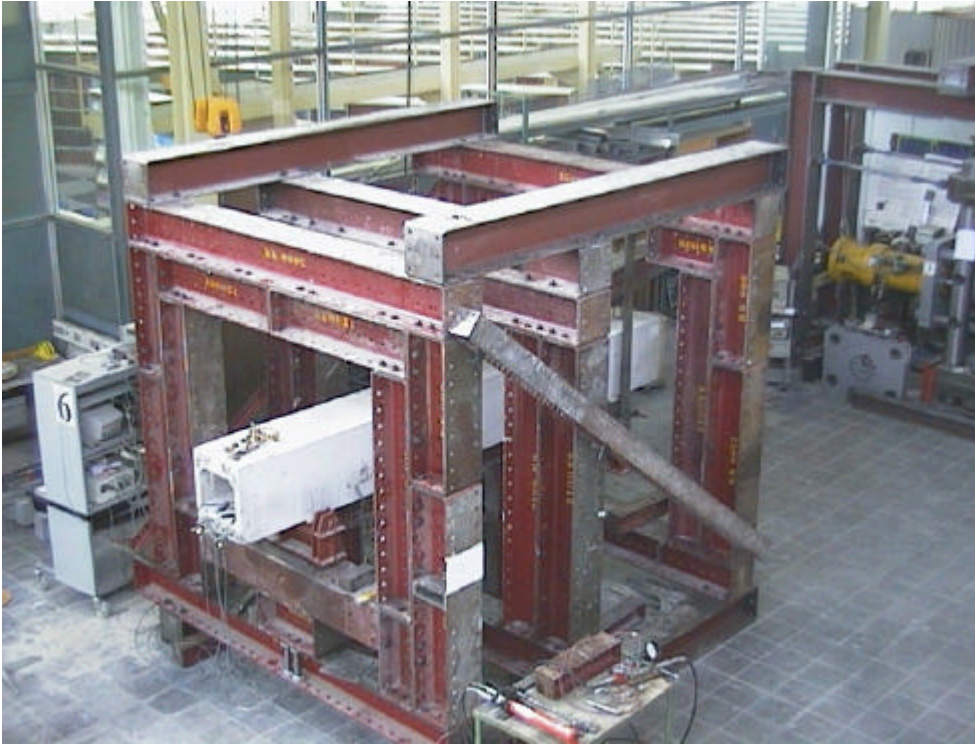


Figure 37 Test arrangements for the shear test on LWAC beams



Figure 38 Test arrangements for the shear test

10.4 Shear force test

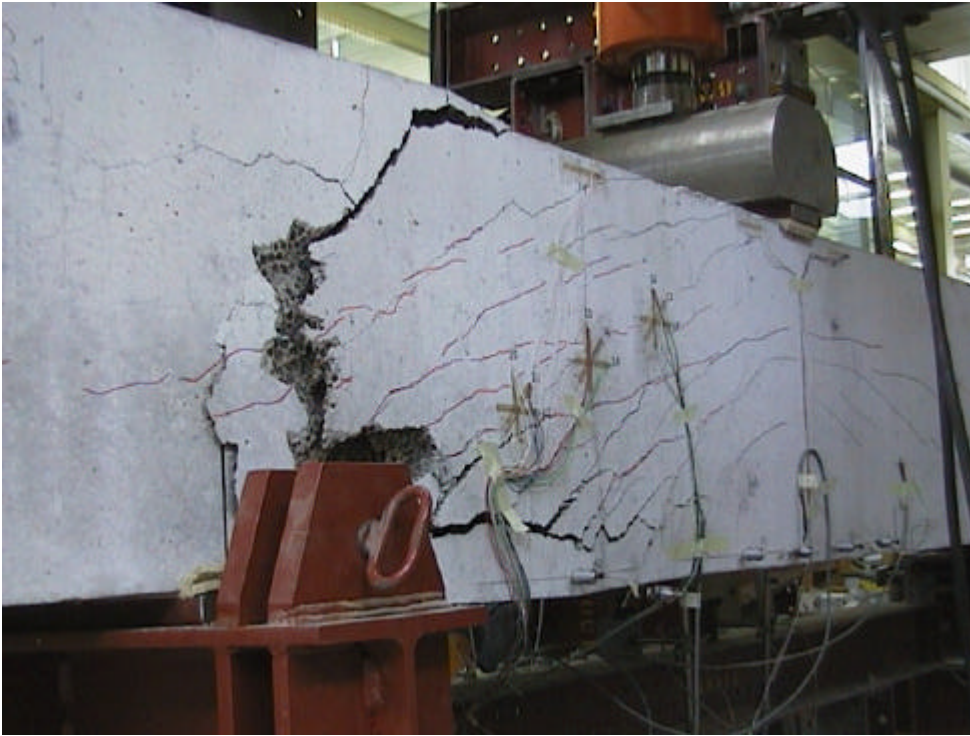
There have been performed 2 shear force tests. In the sequence of loading steps for the test, the cracking and failure mode is shown.

The failure load in shear test	S1LBB1V: 663 kN	Anchorage failure
load	S4LBB2V: 647 kN	Compression failure under the

Test beam S1LBB1V:



The shear capacity of prestressed beams



Test beam S4LBB2V:



The shear capacity of prestressed beams

